



De Geer moraine internal architecture based on sedimentological and geophysical investigations and implications for ice-marginal reconstructions

GWYNETH E. RIVERS , ROBERT D. STORRAR , ANTTI E. K. OJALA , JONI MÄKINEN, CAMILLA HOLMROOS AND NAOMI HOLMES

BOREAS



Rivers, G. E., Storrar, R. D., Ojala, A. E. K., Mäkinen, J., Holmroos, C. & Holmes, N.: De Geer moraine internal architecture based on sedimentological and geophysical investigations and implications for ice-marginal reconstructions. *Boreas*. <https://doi.org/10.1111/bor.12692>. ISSN 0300-9483.

De Geer moraines (DGMs) may act as valuable ice margin indicators; however, to date, their variable mode of formation has presented challenges for this utility. Morphometric investigations provide useful insights into formation processes, which can be developed using sedimentological and geophysical methods. Here we present sedimentological and ground penetrating radar (GPR) data of DGMs located in southwest Finland. Individual lithofacies were identified and interpreted using sediment architectural elements. These were correlated with neighbouring GPR radargrams and extrapolated across the wider study area. Generally, internal architecture presents a multi-phase structure with lower units representing subglacial traction till and ice margin infill deposits, truncated by a larger prominent push unit, which is then successively deformed via the overriding of active ice. Significantly, there are notable differences between proximal and distal structures, with proximal sides characterized by silts, clays, and diamicton with laminae, stratification and thrust planes, and distal sides characterized by poorly consolidated diamicton and proglacial water current reworkings. Internal architecture of both prominent and intermediate ridges is very similar, reflecting similar formation processes, however, slight differences also reflect inter-seasonal variations. Based on our findings, we present an integrated conceptual model for the genesis of DGMs whereby inter-seasonal ridge forming processes occur within a sub-aqueous ice-marginal environment. Our model highlights that DGMs can be subcategorized as: (i) sediment deposition at an unstable margin during summer calving, and/or (ii) sediment pushing at a stabilized margin during a winter re-advance. We do not find evidence of crevasse filling as a mechanism for DGM formation. We propose a landform assemblage classification whereby 'De Geer terrain' is used to describe series of parallel ridges arranged in a typical washboard-like configuration. This classification identifies all DGMs derived within a sub-aqueous ice-marginal environment, whilst also capturing the equifinal characteristics between individual landforms.

Gwyneth E. Rivers (gwyneth.rivers@student.shu.ac.uk) and Robert D. Storrar, *Geography, Environment and Planning, Sheffield Hallam University, Howard Street, Sheffield S1 1WB, UK*; Antti E. K. Ojala, *Department of Geography and Geology, University of Turku, FI-20014 Turku, Finland and Geological Survey of Finland, Vuorimiehentie 5, FI-02151 Espoo, Finland*; Joni Mäkinen and Camilla Holmroos, *Department of Geography and Geology, University of Turku, FI-20014 Turku, Finland*; Naomi Holmes, *Department of Environment and Geography & Department of Education, University of York, York YO10 5DD, UK*; received 2nd July 2024, accepted 3rd December 2024.

Palaeo-ice sheet reconstructions can provide us with valuable information regarding the extent and evolution of past ice sheets (Boulton *et al.* 1984; Dyke *et al.* 2002; Hughes *et al.* 2016; Stroeven *et al.* 2016; Gowan *et al.* 2021; Clark *et al.* 2022). This is important as it enables us to understand how the cryosphere responds to global/hemispheric climate and environmental change, and how glacial ice behaves under different localized conditions. Ice-sheet reconstructions are typically produced by a 'glacial inversion model' (Kleman *et al.* 1997), allowing inferences to be made from the integration between geomorphological evidence, numerical dating and modelling (Clark 1997; Stokes *et al.* 2015; Pearce *et al.* 2017; Gowan *et al.* 2021; Dalton *et al.* 2023). Modern palaeo-ice sheet reconstructions provide time-slice resolutions of between 1000 and 100 years (Hughes *et al.* 2016; Stroeven *et al.* 2016; Clark *et al.* 2022); however, as remotely sensed data improve (e.g. LiDAR derived digital elevation models (DEMs)), it is possible that

lower-relief geomorphology may be identified and used to improve these resolutions.

De Geer moraines (DGMs) are low-relief landforms and can be characterized as long, narrow, elongated ridges that are orientated transverse to the former ice-flow direction. These ridges often occur in swarms, closely spaced, parallel to the ice margin with either regularly spaced and laterally continuous, or irregularly spaced and laterally discontinuous configurations, typically resembling a washboard-like appearance (De Geer 1889; Hoppe 1959; Benn & Evans 2010; Ojala *et al.* 2015; Ojala 2016). DGMs are moderately sinuous and often display asymmetric cross-profiles with a steeper distal side, although symmetric ridges have also been observed (Todd *et al.* 2007; Rivers *et al.* 2023). DGMs commonly occur below the highest shoreline of proglacial lakes/seas (Prest *et al.* 1968; Ojala *et al.* 2015; Ojala 2016). However, observations have also been made in mountainous-valley, lacustrine environments (Golledge & Phillips 2008; Regnéll *et al.* 2023).

Since the first observations in Sweden (De Geer 1889), several conceptual models of DGM formation have been considered, with two overarching hypotheses historically debated. The first constitutes formation at the grounding line of water terminating ice margins (De Geer 1889, 1940; Sollid & Carlson 1984; Sollid 1989; Larsen *et al.* 1991; Blake 2000; Lindén & Möller 2005; Golledge & Phillips 2008; Bouvier *et al.* 2015; Sinclair *et al.* 2018). The second hypothesis can be described as a crevasse cavity infilling process whereby saturated and deformable sediments at the bed of the ice are squeezed up into full depth and/or basal crevasses (Andrews 1963; Strömberg 1965; Zilliacus 1989; Beaudry & Prichonnet 1991, 1995). This crevasse infilling process occurs up ice, behind the grounding line and is similar to the formation process of crevasse-squeeze ridges (CSRs) but presents different spatial patterns (e.g. ‘washboard’ terrain instead of geometric ridge networks) and potentially without the squeezing that is inherent in CSRs (Benn & Evans 2010; Rea & Evans 2011; Evans *et al.* 2016). The morphological similarities between DGMs and CSRs have been the cause of debate regarding DGM origin; however, the hypothesis that DGMs are formed at the grounding line of water terminating ice margins is most widely accepted (Larsen *et al.* 1991; Blake 2000; Golledge & Phillips 2008; Bouvier *et al.* 2015; Rivers *et al.* 2023).

When reviewing DGM formation at the grounding line, different seasonal models have been proposed, with suggestions of ridge formation during winter re-advances and/or during summer retreat (De Geer 1889, 1940; Frödin 1916; Möller 1962; Sollid & Carlson 1984; Larsen *et al.* 1991; Blake 2000; Lindén & Möller 2005; Bouvier *et al.* 2015; Sinclair *et al.* 2018). In the winter model, ridges are constructed via glacial and glaciifluvial deposition and/or settling at the grounding line, and later deformed as the ice margin advances (De Geer 1940; Larsen *et al.* 1991; Blake 2000; Golledge & Phillips 2008; Bouvier *et al.* 2015; Sinclair *et al.* 2018). It should be noted that some authors place less emphasis on push deforming processes, but instead consider DGM formation as lodgement of till at the ice margin during either re-advances or standstills (Sollid & Carlson 1984). In the summer model, ridges are formed by the advection of subglacial sediments to the grounding line during temporary halts in retreat, preferentially driven by calving processes (Lindén & Möller 2005).

Distinction between the different seasonal formation processes is important as they present different implications for grounding line dynamics. A winter re-advance push formation would infer that ridges form on a periodical basis, with ridge interdistances relating closely to annual rates of ice margin retreat (De Geer 1940; Möller 1962; Zilliacus 1981; Larsen *et al.* 1991; Lindén & Möller 2005; Bouvier *et al.* 2015; Sinclair *et al.* 2018). In contrast, ridges formed during summer would depict

irregular patterns associated with a calving ice margin (Frödin 1916; Möller 1962; Zilliacus 1981; Lindén & Möller 2005; Bouvier *et al.* 2015). The cycle of deposition and calving throughout the summer season would likely repeat, allowing several ridges to be constructed within a single year (Zilliacus 1981; Lindén & Möller 2005). Essentially, winter ridges would delineate glacier dynamics associated with mass balance, and summer ridges would be more representative of sporadic grounding line forcing mechanisms such as calving intensity and thinning (Benn *et al.* 2007; Ritchie *et al.* 2008). The summer and winter models are not mutually exclusive, and the potential alternations between winter and summer ridges introduce complexities regarding preservation potential, as ridges constructed during the summer may be overridden or destroyed during a subsequent winter re-advance (Lindén & Möller 2005; Sinclair *et al.* 2018).

The identification of, and distinction between, ‘summer’ and ‘winter’ DGMs has been discussed in previous studies, with suggestions that regularly spaced, high-relief, and laterally continuous ridges represent annual winter re-advances, and irregularly spaced, low-relief ridges denote summer retreat patterns (Möller 1962; Zilliacus 1981; Lindén & Möller 2005; Bouvier *et al.* 2015). The use of LiDAR in recent years has better enabled the distinction between regular and irregular DGM ridges, allowing the complexities in DGM formation to be observed across large areas (Bouvier *et al.* 2015; Ojala *et al.* 2015; Ojala 2016; Rivers *et al.* 2023).

To our knowledge, explicit comparative field investigations between winter and summer DGMs within the same environment do not yet exist. As such, this study aims to explore the internal architecture of DGMs to investigate differences and/or similarities in prominence and regularity, with a view to increase understanding of DGM formation. The existing morphometry studies in southwest Finland provide valuable detailed insights that may be used to elucidate DGM formation (Ojala *et al.* 2015; Ojala 2016; Rivers *et al.* 2023). Rivers *et al.* (2023) found in Finland that the ridge morphology indicated that DGMs are dissimilar to CSRs; however, these findings may be further improved upon with supportive field investigations. As such, this study aims to address two questions: (i) what are the main sediment units within both prominent and intermediate DGMs, and how do these relate to ridge-forming processes, and (ii) does the sedimentology and structure of the exposed ridges allow the various processes suggested above to be distinguished? We aim to improve the current understanding of DGM formation, particularly regarding different formation processes between ridges, and ultimately assess their validity as geochronometric ice-marginal indicators during the Fennoscandian Ice Sheet (FIS) deglaciation.

Study sites and general characteristics of DGMs in southwest Finland

Southwest Finland is a relatively low-relief depositional setting that was completely overridden by the Fennoscandian Ice Sheet (FIS) during the Last Glacial Maximum (~23–21 ka BP) (Svendsen *et al.* 2004; Clark *et al.* 2009; Johansson *et al.* 2011; Hughes *et al.* 2016; Stroeven *et al.* 2016; Lunkka *et al.* 2021). Much of the Earth's crust in Finland was isostatically depressed leaving southwest Finland submerged below sea level during deglaciation. The ice margin position of the FIS during the Younger Dryas ~12.9–11.7 ka BP is particularly well preserved in southeast Finland by the notable Salpausselkä moraines (Glückert 1995; Rainio *et al.* 1995; Tschudi *et al.* 2000; Saarnisto & Saari-nen 2001; Rinterknecht *et al.* 2004). After the Younger Dryas, a rapid retreat led to significant crenulation of the ice margin and the development of several independent ice lobes across Finland (Lunkka *et al.* 2021). Southwest Finland was host to the Baltic Sea Ice Lobe (BSIL), which was further subdivided into the northeastern Loimaa sub-lobe and the remaining southwestern main lobe, which terminated into the Baltic Ice Lake (BIL) (Lunkka *et al.* 2021).

The geographical setting of the southwestern sector of the BSIL is unique in that the interconnected processes between deglaciation, continental rebound, and fluctuating water depths would have imposed significant controls over geomorphological development (Ojala *et al.* 2013; Ojala 2016; Lunkka *et al.* 2019; Fig. 1), resulting in a landscape characterized by abundant DGMs.

A recent study investigated DGM morphometry across southwest Finland (Rivers *et al.* 2023), building on previous studies undertaken by Ojala *et al.* (2015) and Ojala (2016). Morphometrics of both prominent (regularly spaced) and intermediate (irregularly spaced) DGMs were compared to those of typical CSRs located in the Northwest Territories, Canada. The findings revealed statistically significant differences between DGM and CSR morphometries, with DGMs presenting lower-amplitude, more sinuous, and slightly more asymmetric geometries. Importantly, the study highlighted that sinuous and slightly asymmetric cross-profile tendencies support the notion that DGMs located in southwest Finland are formed at the ice margin via unidirectional push processes, rather than via a crevasse cavity squeeze-up process.

Within the same study, Rivers *et al.* (2023) compared the morphometry of prominent (high-relief and regularly spaced) and intermediate DGMs (low-relief and irregularly spaced), finding intermediate DGMs to be lower-relief, less sinuous and more symmetric than prominent DGMs. It was suggested by Rivers *et al.* (2023) that intermediate DGMs could be lower amplitude versions of more prominent DGMs, formed via ice-marginal

push, or formed by alternative processes, such as crevasse infilling behind the grounding line. This reiterates the problem of careful morphometric distinction between DGM ridges of differing geometries and highlights the necessity of further investigation to improve understanding.

In southwest Finland, DGMs vary greatly in their distribution and relief pattern (Zilliacus 1981; Ojala *et al.* 2015; Ojala 2016; Rivers *et al.* 2023). The appearance of DGMs may be configured in one of three ways: (i) only regular prominent ridges, (ii) regular ridges interspersed with irregular/intermediate ridges, or (iii) only irregular ridges (Fig. 2). Generally, size can range between 0.1–3 m height, 4–45 m length, 25–500 m width for prominent DGMs, and 0.1–2.5 m height, 10–200 m length, 4–35 m width for intermediate DGMs (Rivers *et al.* 2023). DGM morphometry is also shown to vary across wider areas highlighting controls such as topography, sediment availability and water depth (Ojala 2016; Rivers *et al.* 2023).

From these starting points, our present sites of specific investigation in southwest Finland are given in Fig. 1. The selection of sites was based on LiDAR DEMs and preliminary field reconnaissance during spring 2023.

Material and methods

Sedimentological and GPR data were acquired at Uimarannatie, Haaro, Perniö (Site (1) in Fig. 1), and independent GPR data were acquired at three additional sites (2, 3 and 4 in Fig. 1). Ridges are identified as either prominent (large and regular ridges) or intermediate (small and irregular ridges) based on the subclassifications of Rivers *et al.* (2023).

Sedimentological investigations

For this study, sediment exposures were obtained via excavations across the mid-sections of one prominent (UT1) and one intermediate (UT2) DGM at Uimarannatie, Haaro, Perniö at right angles to the ridge crestlines (Fig. 3). Vertical sections of the trenches were photographed and logged for lithological units and sediment structural characteristics. Descriptions of vertical sections at UT1 and UT2 trenches were supplemented with site-specific logs: UT1_2023_log1, UT1_2023_log2, UT1_2023_log3, UT2_2023_log4 and UT2_2023_log5, where lithofacies unit characteristics were delineated in more detail. Sedimentological logging of units included grain-size, degree of sorting, matrix composition and clast lithology, with lithofacies codes applied to each unit (Evans & Benn 2004). Altogether, nine clast macrofabric samples (50 clasts, a-axis azimuth and dip) were acquired and plotted in rose diagrams and stereonet using Orient software (Vollmer 2023). In addition, we subsampled different lithological units for grain-size distribution (10 samples from UT1 and six

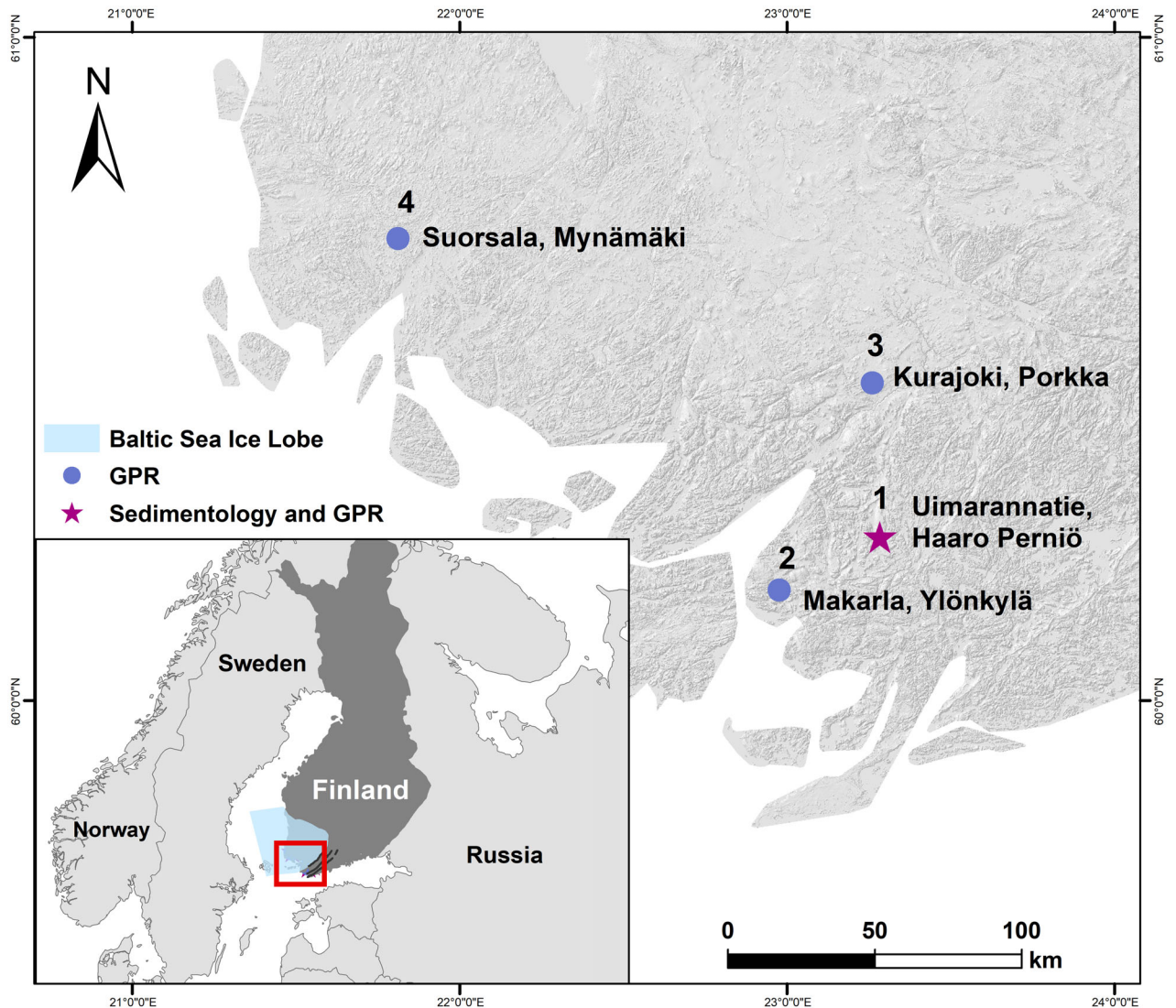


Fig. 1. Location map indicating selected sites across southwest Finland for data acquisition: 1 = Uimarannatie, Haaro, Perniö – sedimentology and GPR; 2 = Makarla, Salo – GPR; 3 = Kurajoki, Salo – GPR; 4 = Suorsala, Mynämäki – GPR. Note the blue area marks the extent of the Baltic Sea Ice Lobe (BSIL) in which the investigated De Geer moraines are located.

samples from UT2) that were dry sieved in the laboratory and measured for grain-size distribution (>0.063 mm) (Figs S5, S6, S11, S12).

Geophysical investigations and radar facies identification

Ground penetrating radar (GPR) has become an increasingly popular approach for investigating the internal architecture of glacial landforms (Neal 2004; Livingstone *et al.* 2017; Stoker *et al.* 2021; Harrison *et al.* 2022; Lally *et al.* 2023). Whilst there is a degree of subjectivity in GPR interpretations, this method provides a valuable alternative and/or supplementary approach to sedimentological analyses whereby the internal architecture of landforms can be investigated non-intrusively and relatively easily, allowing more

representative data sets to be acquired. Subjectivity in interpretation can be overcome by ‘ground truthing’ GPR interpretation with sediment exposures, where possible.

GPR data in this study were collected using a 32-bit MALÅ GroundExplorer (GX) 160-MHz shielded antenna mounted on a rough terrain skid plate and connected to a MALÅ GX controller. Profiles were acquired using a wheel acquisition mode with traces recorded every 0.05 m. A velocity of 0.1 m ns^{-1} was used based on antenna frequency and lithology, providing an estimated penetration depth of ~ 5 m, although this depth will be restricted by the presence of conductive silts and clays (Jol 1995; Jol & Bristow 2003; Livingstone *et al.* 2017; Stoker *et al.* 2021; Lally *et al.* 2023).

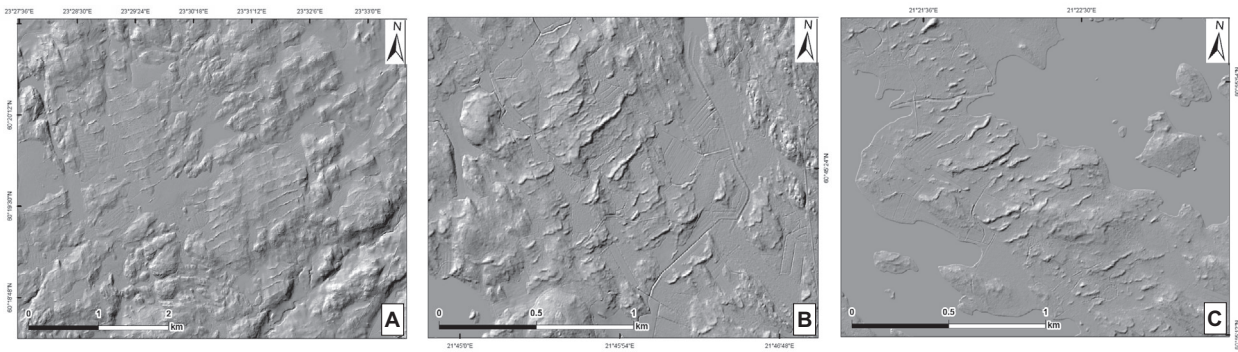


Fig. 2. Hillshaded digital elevation model (DEM) imagery depicting different DGM field types across southwest Finland. A. Kurkela (Salo) – regular, only prominent DGMs. B. Pehtsalo (Laitila) – regular DGMs interspersed with irregular DGMs. C. Pohiperä (Uusikaupunki) – only irregular/more scattered DGMs with a less distinct rhythmic distribution (DEM source: [©]National Land Survey of Finland, LiDAR digital elevation model, 2/2023).

GPR data were processed using REFLEXW v7.5.9 (proprietary software of Karl-Josef Sandmeier). A standard processing sequence, close to those used in similar studies (e.g. Stoker *et al.* 2021; Lally *et al.* 2023), was applied across all profiles. This comprised: static correction of time-zero drift, removal of low frequency signal saturation (DEWOW), application of gain to increase visibility of reflectors at depth, and 3D topographic profile correction. Radargrams were visualized and interpretations were presented using Adobe Illustrator. For transparency, we present unannotated radargrams alongside our interpretations.

Radar facies were determined by identifying variations in reflector motif (e.g. reflector strength, length, shape, amplitude, and pattern). Radar facies were compared with the lithofacies observed in the trenches at Site (1) UT1 and UT2 between the excavated sediment exposures and neighbouring GPR profiles to ensure an accurate basis for GPR interpretation (see Table 1, Figs S1, S7). This was then extrapolated and used to interpret radargrams acquired at the additional locations across the study area, where sediment sections were not available (Fig. 1). It should be noted that we have interpreted facies at Sites (2, 3 and 4) based on the exposures at Site (1). Whilst we can observe similar radar facies between sites, we cannot be certain that the facies at Sites (2, 3 and 4) are directly related to the observed exposures at Site (1). It is possible that there may be other units/facies that are not described from the exposures at Site (1). However, we believe that the exposures at Site (1) provide enough evidence for reasonable interpretation.

Uncrewed aerial vehicle field observations

A high-resolution (7 cm) DEM and orthomosaic of the study area were produced using UAV-based Structure from Motion photogrammetry. A DJI Mavic Pro was used to collect overlapping photographs, and 10 ground

control points, evenly distributed across the area, were surveyed using a Trimble R10 GNSS. Images were processed using Agisoft Metashape v1.8.1 (Agisoft 2022). The orthophoto and DEM were used for field observations and topographic corrections of GPR profiles.

Results and interpretation

Site (1) UT1 (Uimaramantie, Haaro, Perniö (latitude 60°14' N, longitude 23°16' E))

One trench was excavated, and three GPR-lines were acquired at Site (1) UT1 (Fig. 4). The DGM at UT1 is a large, prominent ridge, ~485 m long, ~2 m high and ~40 m wide. It should be noted that the sediment exposure did not reach bedrock; however, GPR data were used to identify this. The logged sections (Fig. 5) and sediment exposure combined with the GPR profiles (Table 1, Figs S1–S4) revealed five main lithofacies:

Unit 1 sits within the distal regions, at the base of the ridge, likely overlying till-covered bedrock, as identified by GPR. Interpreted steep thrust planes dip up-ice, toward the proximal side of the ridge. Hyperbolic diffractions and parallel to subparallel reflectors suggest stratified deposits interspersed with boulders (Table 1 RF1, Fig. 6 Unit 1).

Unit 2 is located on the distal side of the exposure (Fig. 5); however, based on our radar facies interpretation it stretches across to the proximal side of the ridge. This unit was only partially exposed, with the majority only observable in the radar profile. We interpret the unit to range from horizontal and deformed laminated sands, to massive gravel and medium to coarse-grained sands, interspersed with silt, fine-grained sands and granular gravel lenses. The radar profile shows steep dipping reflectors, which may represent thrust planes. This unit is truncated and deformed with a diffuse upper contact boundary to Unit 3.

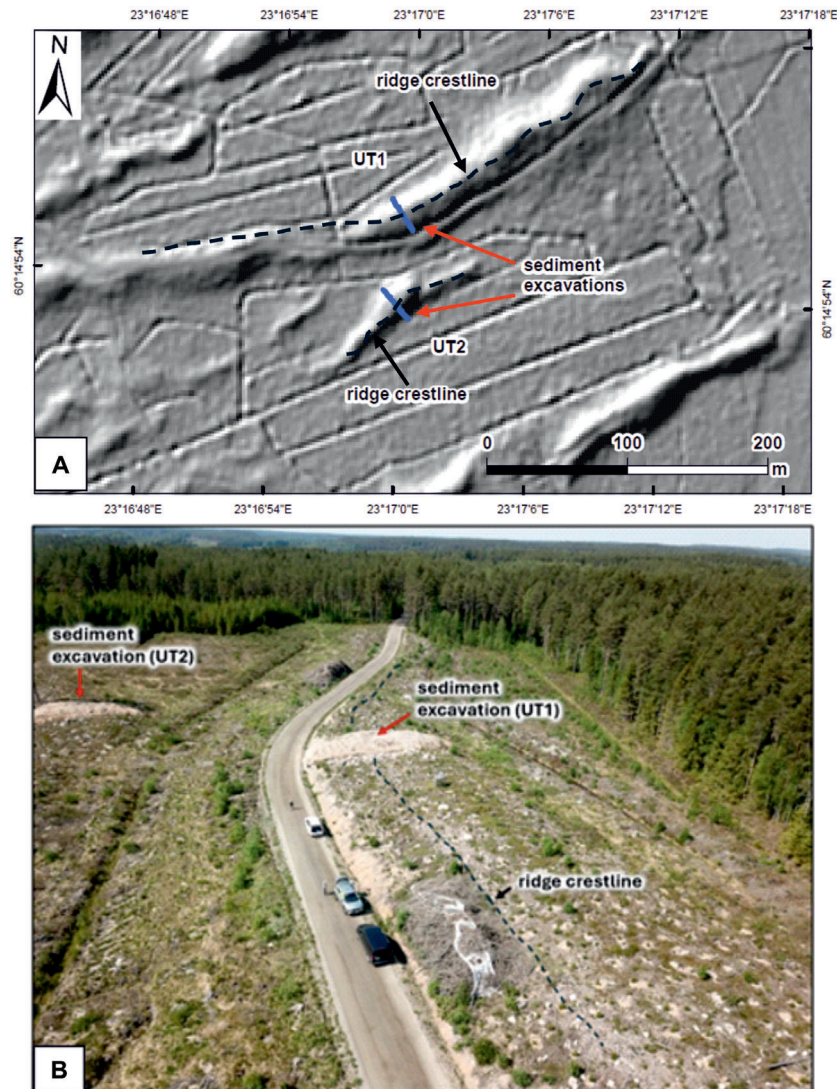


Fig. 3. Location of excavated sediment exposures at Site (1) Uimarannatie, Haaro, Perniö (see Fig. 1). A. Hillshaded DEM highlighting prominence of DGMs and positioning of sediment excavations. B. Oblique photograph of excavated sediment exposures facing southwest.

Unit 3 comprises most of the ridge morphometry (Figs 5, 6) and is divided into two subunits: Unit 3a, located in the proximal part of the ridge and Unit 3b, located within the distal part. Unit 3a can be defined as poorly sorted massive to matrix-supported diamicton containing weak laminations. The supporting matrix is composed mainly of silt and medium to fine-grained sands. Clast morphology is variable, with clasts ranging from subangular to subrounded. Medium-angle ($330^{\circ}/20^{\circ}$) thrust plane structures are present and dipping in alignment with slope direction (i.e. up-ice). Fissility is well developed particularly in the upper part of the unit. Unit 3b is generally similar to proximal unit 3a; however, DEM contrasts with down-slope dipping low-angle shear structures. The unit shows weak fissility; however, this improves over large clasts. The unit is

interspersed with patches of sand and contains elongated rafts of compact sediment.

Unit 4 drapes the entire ridge with a sharp lower contact boundary to the underlying Unit 3. Its composition ranges from massive to laminated silts and clays, to a sandy, fine-grained diamicton. The unit shows strong shearing aligned to the direction of ice flow (Fig. 7B). The proximal side of the unit is composed of laminated to massive deformed silty clay, separated by a wedge of coarse sand and gravel (Fig. 7B). This then transitions to sandy, fine-grained diamicton characterized by laminae (lenses of fine to medium sand) interspersed with pebbles. The orientation of pebble clasts follows laminae structures that conformably overlie gravel clasts. Gravel clasts are mainly subrounded. The upper contact boundary is mainly diffuse, although sharp/erosional in some places.

Table 1. Summary of interpreted radar facies based on correlations with UT1 and UT2 lithofacies as presented in Figs S1, S7.

Radar facies no.	RF example	Reflector motif	Correlated lithofacies	Lithological description
4		Long and continuous with high reflectivity. Parallel to subparallel and slightly wavy arrangement.	4	UT1: Fld, Fmd, Sld, Dms UT2: Sld, Dms
3a		Medium to long, with medium continuity. Medium to weak reflector strength with parallel to subparallel arrangement.	3a	Dmm, Dml
3b		Short to medium in length with medium continuity to discontinuous. High to medium reflectivity. Wavy and sometimes overlapping.	3b	UT1: Dmm, Dml, Dcs UT2: Dcs, Gcs
2		Medium to long, with medium continuity, although sometimes discontinuous. Strong reflectivity with parallel to subparallel arrangement.	2	UT1: Sld, Smd, Gs UT2: Sld, Smd, (g)Smd, Gs
1		Very short, very discontinuous with high to medium reflectivity. Wavy, sometimes overlapping with hyperbolic diffractions. Interpretation of coarse diamicton with boulders.	1	Unknown. Not exposed within sediment excavation; partly exposed in UT2. Hyperbolic diffractions may suggest coarse, poorly sorted, bouldery diamicton, or fractured bedrock.

Unit 5 is the uppermost unit, mantling the ridge. The unit is composed of massive to matrix-supported sandy diamicton, clast-rich, with boulders, and containing crude clast layers (one clast thick). The unit thickens down-slope on the proximal side. The lower proximal slope comprises massive medium to very coarse sand, interspersed with granule lenses and pebbles. In the upper parts, this passes into a loose massive to matrix-supported sandy gravel and medium to coarse-grained sand. Clasts are mainly rounded to subrounded. GPR data show similar structures across all acquired profiles from this ridge. In particular, interpreted sheared structures within RF3a and RF4 are distinctive features in the upper parts of the radar profiles as indicated by long and continuous reflectors, representing lithofacies Units 3a and 4.

Unit 1 is interpreted as a buried bouldery sediment ridge with proximal thrust planes, overlying till-covered bedrock. This unit forms the core of the De Geer ridge. Similar ridge-like architecture can be seen in some of the GPR profiles from the Uimarannatie site (Figs S2–S4).

Unit 2 is interpreted as glacialfluvial material, deposited either at the ice margin or behind the ice margin via

shallow distributed canals as suggested by composition, degree of sorting and presence of laminations (Bennett *et al.* 2000; Bennett & Glasser 2009). The presence of steep thrusting structures at the root of the ridge suggest deformation by ice movement either syn-depositionally and/or during the later stages of ridge bulldozing (e.g. formation of Unit 3a).

Units 3a/b are interpreted as the main body of the ridge whereby coarser subglacial material is deposited via bulldozing at the grounding line. An initial subglacial origin of the material is supported by clast form (e.g. subangular to subrounded; Benn & Ballantyne 1994). The pushing/bulldozing of this material is evidenced by the presence of compressional up-ice dipping thrust planes and compact fissile textures located within the proximal regions of the unit (e.g. Unit 3a; Evans *et al.* 2006).

Unit 4 is characterized by strong shearing structures and a distinct clast orientation to ice-flow direction indicating overriding of ice. The extent of overriding may vary, potentially overriding only as far as the ridge crestline as suggested by Lønne & Nemeč (2011).

Unit 5 is interpreted as basal till that has melted out from the bottom of the ice during the final melting of the

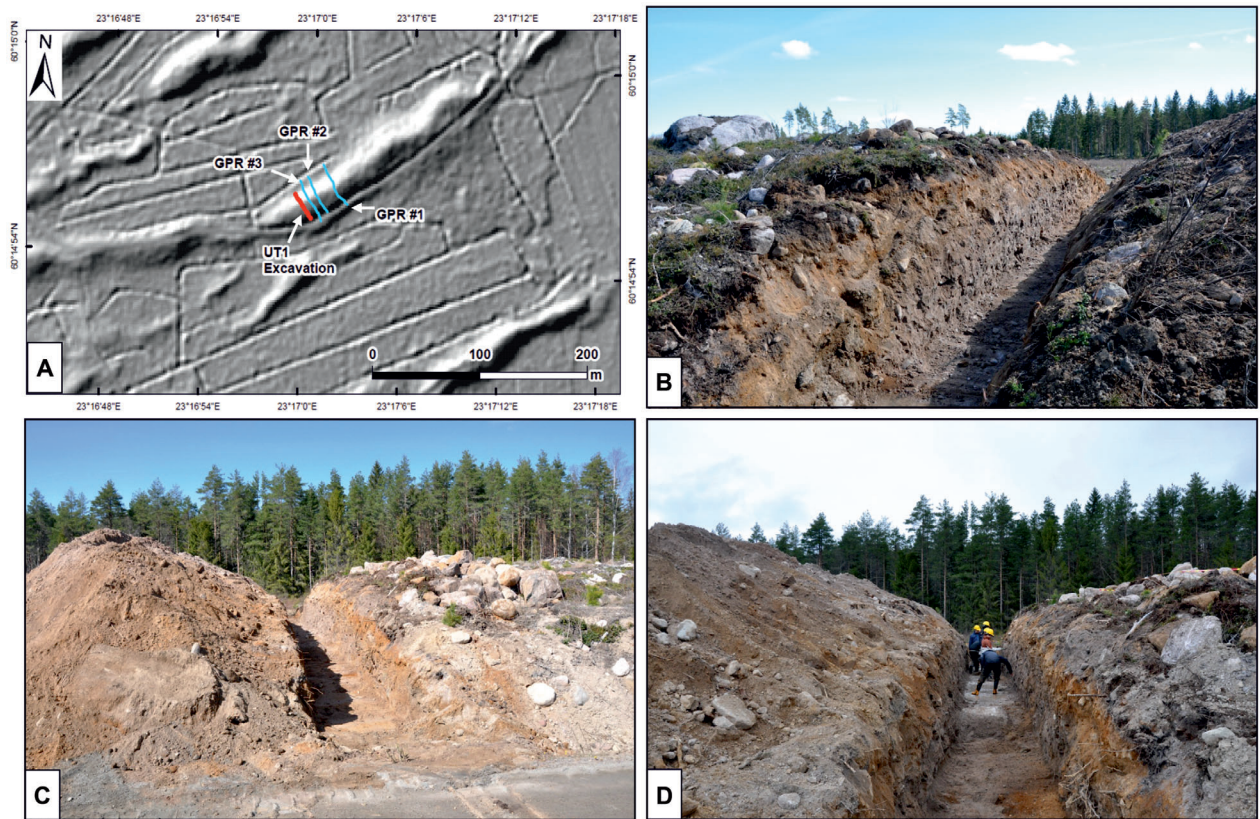


Fig. 4. Imagery of UT1 excavated sediment exposure. Excavation dimensions: length ~28 m; depth ~2 m. A. Hillshaded DEM indicating location of sediment exposure and GPR profiles along UT1 ridge at Site (1) (DEM source: ©National Land Survey of Finland, LiDAR digital elevation model, 2/2023). B. Photograph viewed from proximal to distal. C. Photograph viewed from distal to proximal. D. Photograph viewed from distal to proximal.

ice sheet. This has been subsequently reworked by shore sedimentation and proximally transitions to beach deposits. This material is also modified by frost heave, root zone and soil development but the exact process is not clear. This type of diamicton is also typical for murtoos and exists in areas not influenced by shoreline processes (Mäkinen *et al.* 2023).

Site (1) UT2 (Uimaramantie, Haaro, Perniö (60°14' N, 23°16' E))

One trench was excavated, and three GPR-lines were acquired at Site (2) UT2 (Fig. 8). The DGM at UT2 is a lower amplitude, intermediate ridge, ~100 m long and ~25 m wide. The sediment exposure revealed five main lithofacies units (Figs 9, 10).

Unit 1 is located at the base of the ridge and comprises matrix-supported massive diamicton with large boulders (only the upper surface of the unit was exposed). This unit is likely overlying bedrock.

Unit 2 is situated on top of Unit 1 in the distal part of the ridge. This unit comprises stratified massive gravel and medium to coarse-grained sand (clast form sub-

angular to subrounded), mantled by boulder clast horizons. Partly preserved patches of silty, fine-grained sand were observed in the lowest part of the unit. The unit is thicker and more prominent compared to a similar unit at Site (1) UT1.

Unit 3 is situated across the entire ridge and truncates Unit 2 with an erosional to diffuse and deformed contact boundary (Fig. 11A). This unit is sub-classified into Units 3a and 3b, whereby Unit 3a is located toward the proximal regions of the ridge, and Unit 3b is located toward the distal side. Unit 3a is composed of massive/matrix-supported and laminated diamicton. The matrix is poorly sorted silt and fine to coarse-grained sand. Clasts are subangular to subrounded. This unit contains steeply dipping thrust planes (some nearly vertical; Fig. 9) and sediment rafts/blocks. The lower part contains pebbly sand beds (~5 cm thick). This unit is grey in colour and showed weak fissility in places. Unit 3b comprises clast-supported, stratified diamicton and gravel. This unit also contains large boulders/a boulder horizon, and patches of sand with down-slope dipping crude bedding (Fig. 11B). In contrast to the proximally located Unit 3a, this unit has a higher sand/gravel

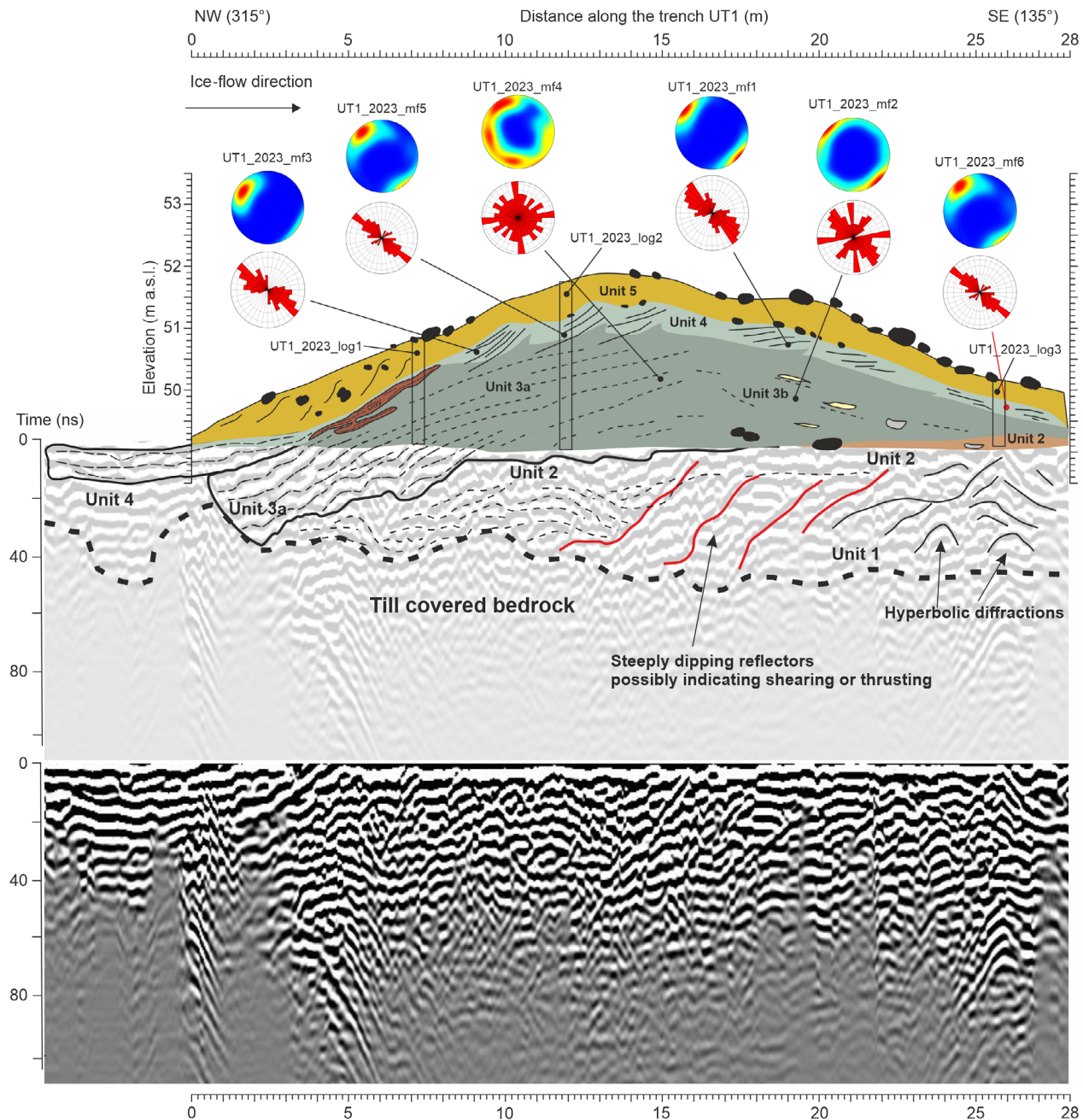


Fig. 5. Exposure sketch of UT1 with the original subsurface (bottom) and interpreted (middle) GPR data. GPR data were acquired along the excavation bottom to allow subsurface investigations. Locations of sediment logs are shown (e.g. UT1_2023_log1, UT1_2023_log2 and UT1_2023_log3), which are presented in Fig. 6. Locations of clast macrofabric measurements are indicated, with data presented in rose diagrams and stereonets. Stereonets are plotted on the lower hemisphere of a Schmidt diagram. Lithofacies units are labelled accordingly and presented in sediment logs shown in Fig. 6.

content, a higher degree of sorting, and is light grey to yellow in colour.

Unit 4 is situated in the proximal to central regions of the ridge and overlays Units 3a/b with a diffuse and deformed contact boundary. Material comprises horizontal/draped laminated sands and diamicton. Significant shearing structures are present, similar to

those observed in Unit 4 UT1; however, these are only present in the proximal part of the ridge (Fig. 9).

Unit 5 mantles the entire ridge, overlying Units 4 and 3b with sharp, erosional contact boundaries. This unit shows similarities to Unit 5 in UT1, comprising clast-supported massive gravel and matrix-supported massive diamicton, with shearing structures.

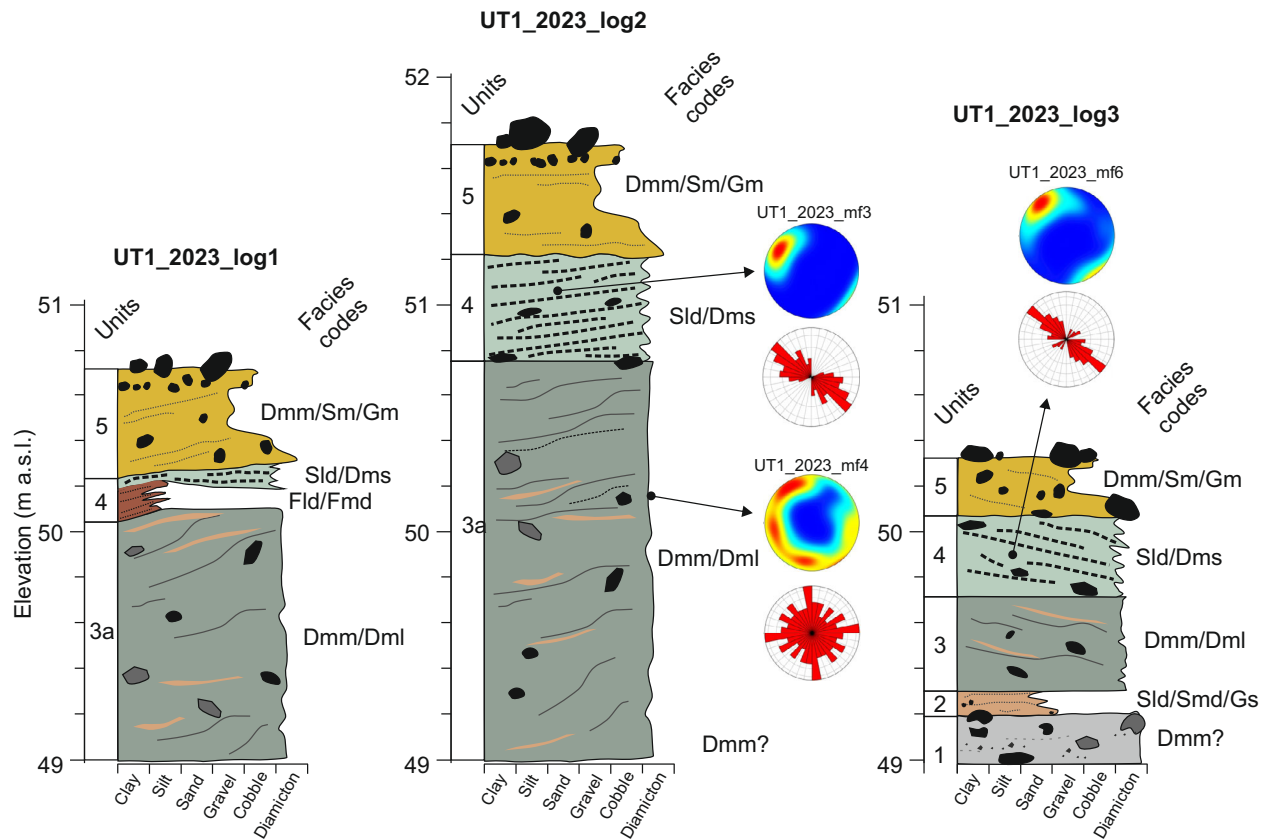


Fig. 6. Sediment logs presented from UT1 showing unit thickness, composition and internal structures. Lithofacies are interpreted using standardized coding (Evans & Benn 2004). Rose diagrams and stereonets supplement identified units where applicable. Lithofacies codes: Dml = matrix-supported, laminated diamiction; Dmm = matrix-supported, massive diamiction; Dms = matrix-supported massive diamiction with shearing structures; Fld = fine laminated silt and clay often with minor fine sand and very small ripples and with dropstones; Fmd = massive silt and clay with dropstones; Gmm = massive gravel; Gs = gravel with shearing structures; Sld = horizontal and draped laminated sand with dropstones; Sm = massive sand; Smd = massive sand with dropstones.

Additional radargrams acquired at UT2 highlight some internal variations across the ridge. GPR Profiles #1 and #3 (Figs S8, S10, respectively) show what we interpret to be thrust planes within the proximal part of the ridge. In contrast, Profile #2 (Fig. S9) shows less evidence of thrusting, although some interpreted stratification can be seen.

We interpret Unit 1 to be subglacial till overlying bedrock.

Unit 2 is interpreted as glaci-fluvial material, originally deposited either at or behind the grounding line and/or in crevasses behind the grounding line via distributed or channelized subglacial flow. The mantling boulder clast horizons may represent a sediment horizon deposited



Fig. 7. A. Depositional units from the middle part of UT1 excavation. This shows the main ridge composition of the silty-to-sandy diamiction Unit 3a, which is draped by the fine-grained and highly fissile/sheared Unit 4. Unit 5 forms the mantle of the ridge composed of bouldery diamiction. B. Strongly sheared and fissile structures of Unit 4. C. View toward the proximal section of the UT1 De Geer ridge. Note the deformed clay layers between Units 3a and 5. White arrows indicate ice-flow direction.

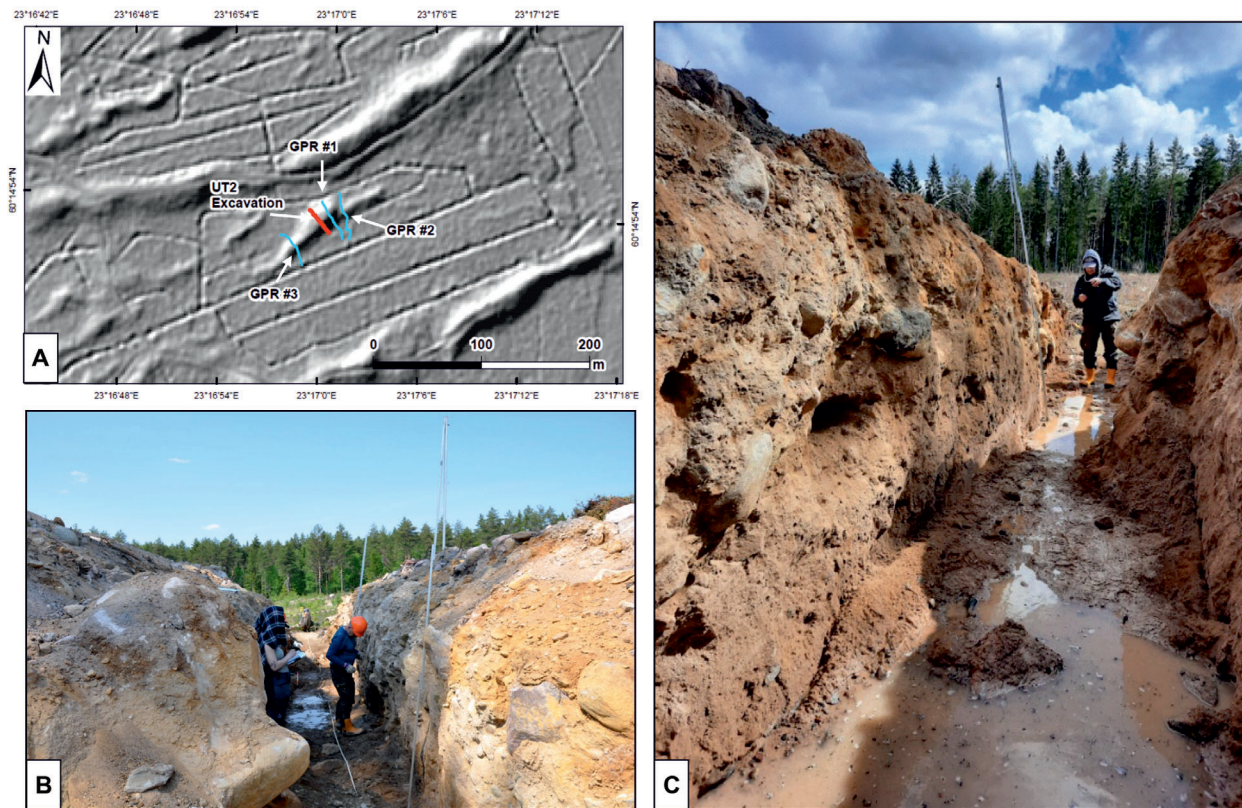


Fig. 8. DEM and photographs of UT2 excavated sediment exposure. Excavation dimensions: length ~28 m; depth ~2 m. A. Hillshaded DEM showing location of sediment exposure and GPR profiles along UT2 ridge at Site (1) (DEM source: ©National Land Survey of Finland, LiDAR digital elevation model, 2/2023). B. Photograph viewed from distal to proximal. C. Photograph viewed from proximal to distal.

during downwasting of surrounding ice or could be related to erosional lag affected by deformation processes. Also, this unit is subsequently deformed by proximal (and/or submarginal) thrusting likely caused by stress exerted by moving ice. This is supported by the presence of thrust planes and steeply dipping clast orientations in the proximal part of the ridge, combined with sediment rafts.

Unit 3 is interpreted as the main body of the ridge and is subdivided into Units 3a (proximal) and 3b (distal). The high silt content and presence of laminations in the proximal side (Unit 3a) likely reflect the settling out of suspended fine-grained material at the grounding line during a short quiescent phase, which is then later deformed during the onset of ice activity. We interpret that the coarser distal side sediments (Unit 3b) were deposited from beneath the ice at the grounding line into the basin with currents (Golledge & Phillips 2008; Bennett & Glasser 2009; Lønne & Nemec 2011).

Unit 4 is interpreted as ice-marginal deposits subsequently deformed by ice advance, a similar origin to that of UT1, as evidenced by the highly variable matrix composition and significant shearing structures.

Unit 5 is interpreted as basal till reworked by shore processes and proximally replaced by beach deposits, similar to that of UT1. This unit also shows modification by frost heave, root zone and soil development.

The internal variations observed along the ridge (Figs S8–S10) appear to coincide with ridge amplitude as shown in the hillshaded DEM (Fig. 8A). GPR profiles #1 and #3 (Figs S8, S10, respectively) are situated within larger sections of the ridge, where interpreted thrust/shearing planes are observed, whereas profile #2 (Fig. S9) is situated along a smaller section that shows comparatively less evidence of thrusting/shearing. It may be that the ridge comprises two separate formations, whereby the larger section of the ridge overrides a previously formed smaller ridge. This may explain the origin of the lower Units 1 and 2.

Site (2) Makarla, Ylönkylä (60°10' N, 22°58' E)

GPR results are presented for Site (2) below. DGMs in this area can be characterized as large prominent ridges interspersed with smaller, intermediate ridges. The DGM observed is identified as a prominent ridge with metrics of ~300 m long, ~33 m wide and ~1.56 m high. Along

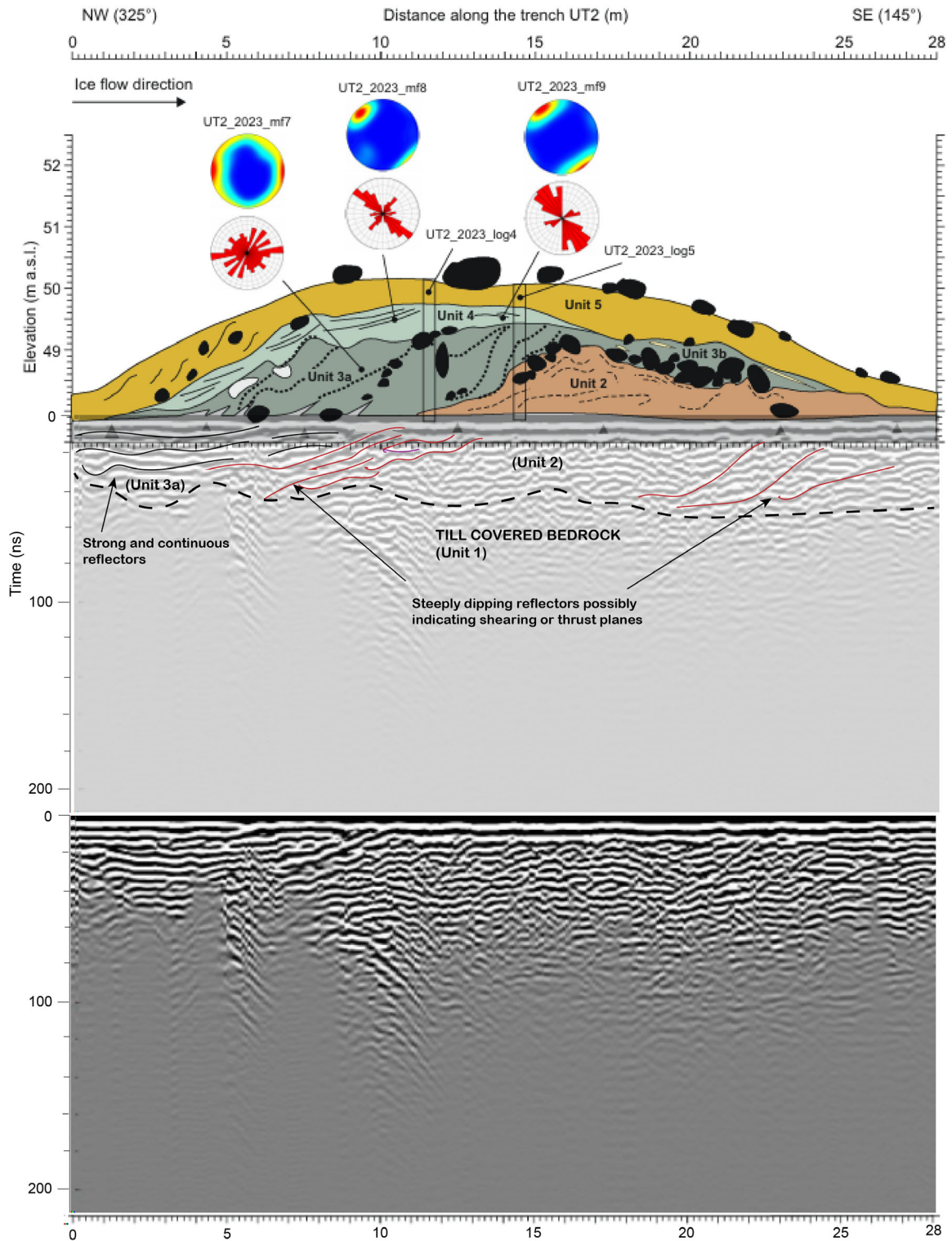


Fig. 9. Exposure sketch of UT2. Locations of sediment logs are shown (e.g. UT2_2023_log4 and UT2_2023_log5); logs are presented in Fig. 10. Clast macrofabric measurement locations are indicated with data presented in both rose diagrams and stereonet (clast macrofabric sample sizes = 50). Stereonets are plotted on the lower hemisphere of a Schmidt diagram. Lithofacies units are labelled accordingly and described in the sediment logs as presented in Fig. 10.

ridge locations for acquired GPR profiles are presented in Fig. 12. GPR data are presented in Fig. 13 (additional radargrams are available in Figs S13, S14).

Proximal regions of the ridge are strongly dominated by RF4 and RF3a, providing evidence of what we interpret to be compaction/laminae and thrusting/shearing that was described in both the UT1 and UT2 excavations. Parallel alignment of reflectors may also signify sequences of stacked sediments. RF3b is located within the distal regions and RF2 and 1 are located at the distal foot of the ridge, containing hyperbolic diffractions that we interpret as the presence of boulders. The coarseness of these distal units may signify gravity driven flow deposits and/or current reworkings whereby finer sediment is removed and coarser material is deposited (Bennett & Glasser 2009). This ridge shows characteristic structures of a grounding line/push depositional process (Bennett & Glasser 2009; Lønne & Nemeč 2011).

Site (3) Kurajoki, Porkka (60°28' N, 23°15' E)

GPR results are presented for Site (3) below. DGMs in this area comprise regular, prominent ridges interspersed with irregular, intermediate ridges. The DGM observed is identified as a prominent ridge due to lateral continuity

and regularity between ridges within the wider terrain; however, this ridge is the lowest amplitude of all observed ridges with metrics of ~745 m long, 1.06 m high and ~24 m wide. Along ridge locations for acquired GPR profiles are presented in Fig. 14. GPR data are presented in Fig. 15 (additional radargrams are available in Figs S15, S16).

The radar facies architecture is different when compared to those previously presented. The ridge is generally overlain by a veneer of long and continuous reflectors (RF4), which may be interpreted as compaction and/or laminations and shearing across the upper part similar to Unit 4 in the UT1 excavation; however, there appears to be little evidence of thrusting structures within the proximal regions. Instead, there appears to be what could be interpreted as the remains of a pre-existing ridge or hummock of coarse, poorly sorted, boulder-filled material within the proximal side, against the interpreted bedrock, as suggested by short, wavy, discontinuous reflectors and hyperbolic diffractions (RF1 and 2), sandwiched between a looser diamicton (RF3b). The upper distal part shows strong evidence of compaction/stratification by long and continuous reflectors (RF4), which may be interpreted as shearing from the deposits being completely overridden by ice. Silt and clay are present throughout most of the ridge, as

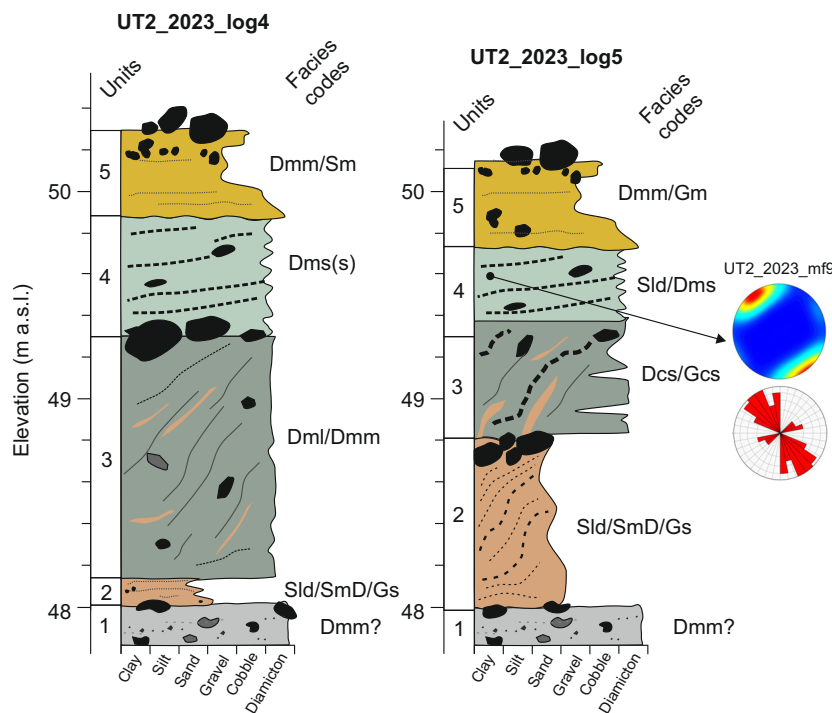


Fig. 10. Sediment logs presented from UT2 showing unit thickness, composition and structures. Lithofacies are interpreted using standardized coding (Evans & Benn 2004). Rose diagrams and stereonets accompany identified units where applicable. Lithofacies codes: Dcs = clast-supported stratified diamicton; Dml = matrix-supported laminated diamicton; Dmm = matrix-supported massive diamicton; Dms(s) = matrix-supported massive diamicton with shearing structures; Gcs = clast-supported gravels with shearing; Gs = gravel with shearing structures; Sld = horizontal and draped laminated sand with dropstones; Sm = massive sand; SmD = massive sands with dropstones.



Fig. 11. A. Depositional units from the middle section of UT2 excavation. Note the deformed, sandy sorted sediments of Unit 2 truncated by Unit 3a that forms the main part of the proximal side of the ridge. B. Down-slope dipping bedding structures in distal parts of Unit 3b. C. Strongly sheared and fissile structures of Unit 4, similar to UT1, but present only in proximal parts of UT2. White arrows indicate ice-flow direction.

indicated by strong signal attenuation. When examining the ridge structure, it seems to follow the orientation of the bedrock. Sediments distal to the bedrock knob are different to the proximal ones indicating a strong influence of bedrock over grounding line processes. As signal attenuation is particularly strong in this profile, it is difficult to form an accurate architectural assessment; however, we can observe that the bedrock has affected DGM formation in this area.

Site (4) Suorsala, Mynämäki ($60^{\circ}42' N$, $21^{\circ}48' E$)

GPR results are presented for Site (4) below. DGMs in this area comprise prominent ridges interspersed with intermediate ridges. The DGM observed is identified as a prominent ridge with metrics of ~ 454 m long, ~ 2.04 m high and ~ 25 m wide. Along ridge locations for acquired

GPR profiles are presented in Fig. 16. GPR data are presented in Fig. 17 (additional radargrams are available in Figs S17, S18).

The proximal regions of the ridge comprise a combination of RF3a and RF3b as detected in the UT1 excavation, with some longer, continuous reflectors in the upper parts that we interpret as compaction/shearing. The alternations between RF3a, representing thrusting, and 3b, representing looser diamicton, infer a more gradual/staggered ice-marginal push process. The distal side of the ridge comprises parallel to subparallel reflectors dipping in the direction of ice flow. Similarly to all other ridges, signal attenuation within lower regions is observed indicating high water, silt and/or clay content. We interpret this ridge to be a typical ice-marginal push formation, comparable to UT1, however, formed in two stages before the formation of Unit 4.

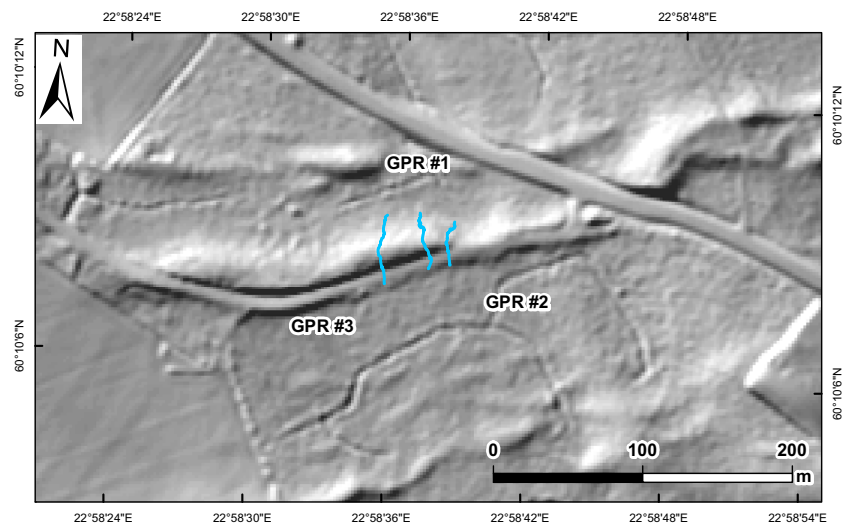


Fig. 12. Hillshaded DEM showing position of GPR profiles along surveyed ridge at Site (2) (DEM source: [®]National Land Survey of Finland, LiDAR digital elevation model, 2/2023).

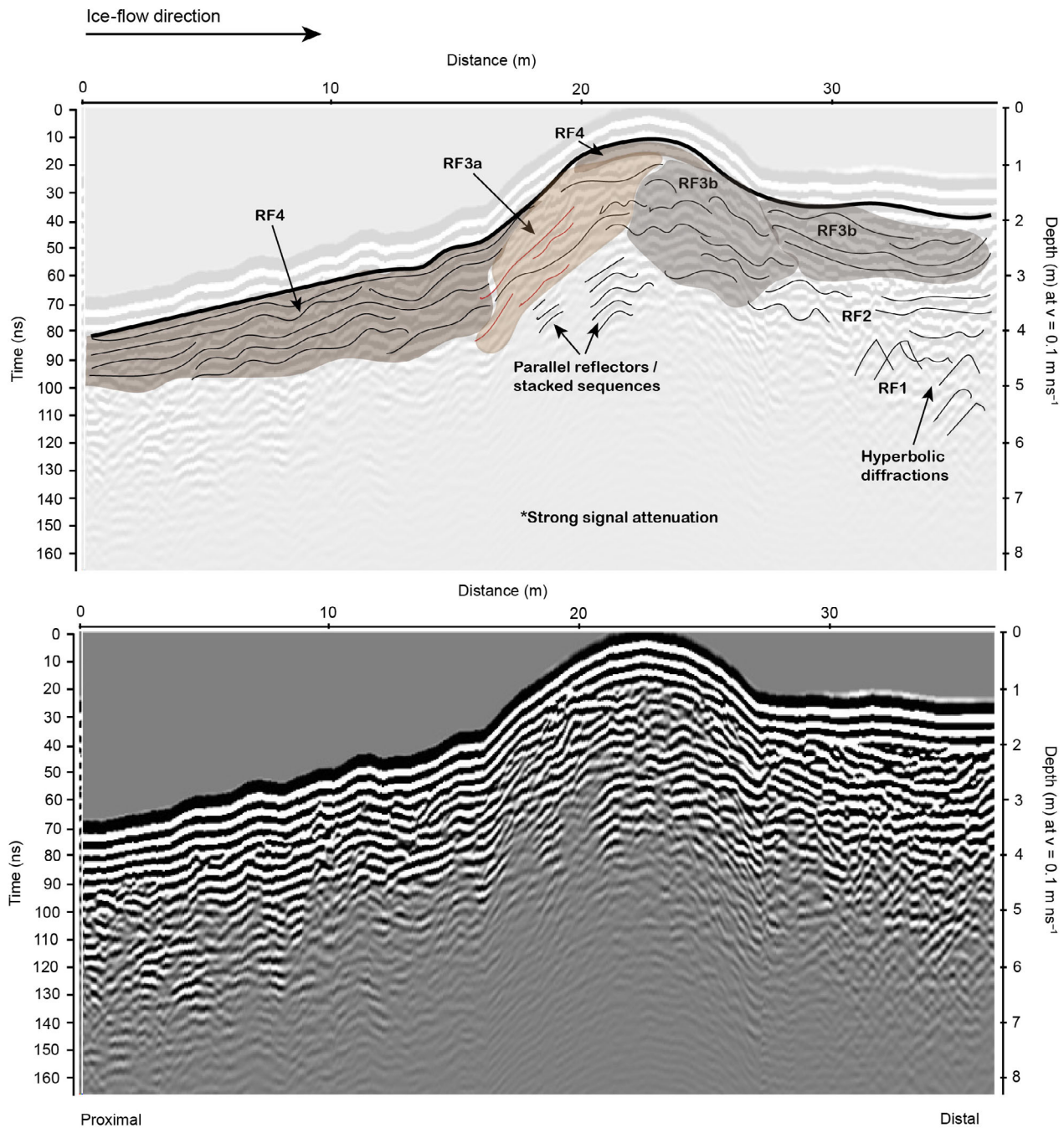


Fig. 13. Radargram #1 at Makarla, Ylönkylä (GPR profiles #2 and #3 are presented in Figs S13, S14). Identified radar facies and connected lithofacies are detailed in Table 1.

Discussion

DGM internal architecture

Our findings show that both larger, prominent and smaller, intermediate ridges comprise the same sediment facies and architectural structures; however, slight variations can be observed. The main insights can be confined to:

- Lower Units 1 and 2 are composed of either buried bouldery ridges with deformed sediments showing proximal thrust plane structures (Site (1) UT1, Unit 1) or basal till (Site (1) UT2, Unit 1) and glaci-fluvial sand/gravel interpreted as waterlain deposition either at the ice margin during summer, or possibly via shallow distributed canals up ice of the margin (Unit 2). Generally, thrusting structures are located within the proximal- to mid-sections of the ridges (Unit 3a);

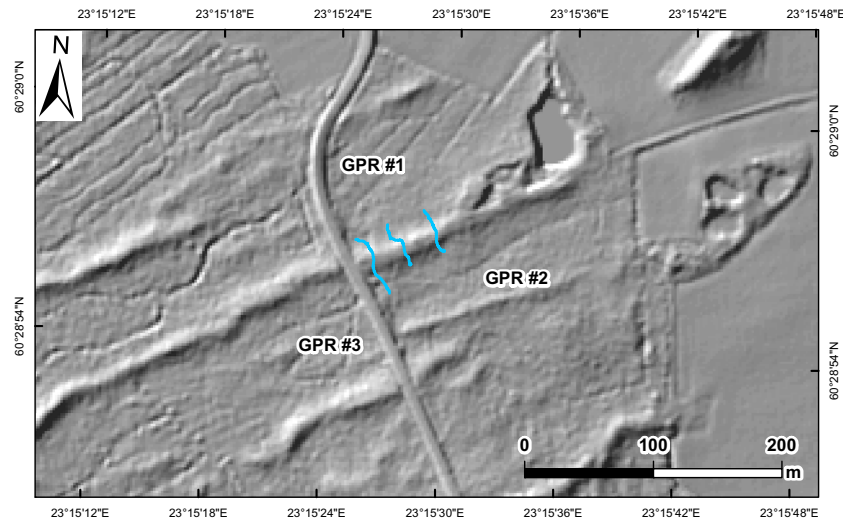


Fig. 14. Hillshaded DEM showing position of GPR profiles along surveyed ridge at Site (3) (DEM source: ©National Land Survey of Finland, LiDAR digital elevation model, 2/2023).

however, these structures are also observed within the lower Units 1 and 2 of UT1 (Fig. 5). These structures may be formed syn-depositionally, or postdepositionally during the formation of Unit 3a. If formed syn-depositionally, this may infer that material was deposited subglacially in crevasse cavities behind the grounding line via shallow distributed canals, which was then overridden by ice and later amalgamated at the grounding line as the ice margin retreated and aligned with the original deposits. The height and prominence of Unit 2 in the UT2 ridge compared to the UT1 ridge are the main architectural differences that we have observed between intermediate and prominent DGMs, in addition to the deformed and rafted clays in the proximal part of UT1 that were likely deposited during a quiescent period in winter (Figs 5, 7C). Furthermore, Unit 2/RF2 may not always be present (see Site (1), UT2, GPR #2 and #3, Figs S9, S10), or may be very thin, possibly mixed with the overlying Unit 3 and therefore not easily identifiable within the GPR data. Without being able to make observations within exposures, it is difficult to make any accurate interpretations.

- Units 3a/b constitute most of the ridge and are interpreted as a grounding line push/bulldozing material. This is particularly notable from proximally located clay slabs pushed onto the ridge (Figs 5, 7C) and from transitions between compression structures in the proximal side and coarser material in the distal part (Lønne & Nemeč 2011). As such, irrespective of the origin of the lower Units 1 and 2 (e.g. basal cavity, subglacial meltwater, or grounding line deposits), Units 3a/b represent a true grounding line formation and therefore support the idea that DGM ridges may be used as ice-marginal indicators.

- Unit 4 is indicative of overriding active ice, evidenced by strong shearing structures at the surface. We suggest that this unit in both UT1 and UT2 has a similar origin, whereby meltwater flow becomes limited, and deposition of fine-grained sediments takes place, while ice continues to retreat at the margin. Note the deformed winter clays associated with this unit in UT1 indicate ice-flow reactivation in spring over the ridge. Differences in unit extent between UT1 and UT2 suggest variability in the extent of ice advance, e.g. overriding ice may extend only as far as the ridge crest as shown in UT2, and are dependent upon factors such as ice thickness and water depth (Lønne & Nemeč 2011). Good preservation of ridges suggests that ice is unlikely to advance significantly beyond the ridge crest.
- Unit 5 can be interpreted as basal till that has melted out from the bottom of the ice during the final melting of the ice sheet. This diamicton has then been washed by littoral processes and modified by frost heave and root zone development (Mäkinen *et al.* 2023).

When comparing internal architecture between the presently studied ridges, it appears that the prominence of thrusting and shearing structures positively correlates with ridge amplitude where the ridges with greater relief (e.g. prominent ridges) show more evidence of thrusting. Furthermore, lower amplitude ridges (e.g. the observed ridge at Site (3); Figs 15, S15, S16) appear to comprise mostly coarser-grained material and present less evidence of stratification and shearing characteristics. These between-ridge variations may denote the seasonal stage at which the deposits were made, as well as the availability and type of material being pushed at the margin, and the prominence of bedrock controls. For

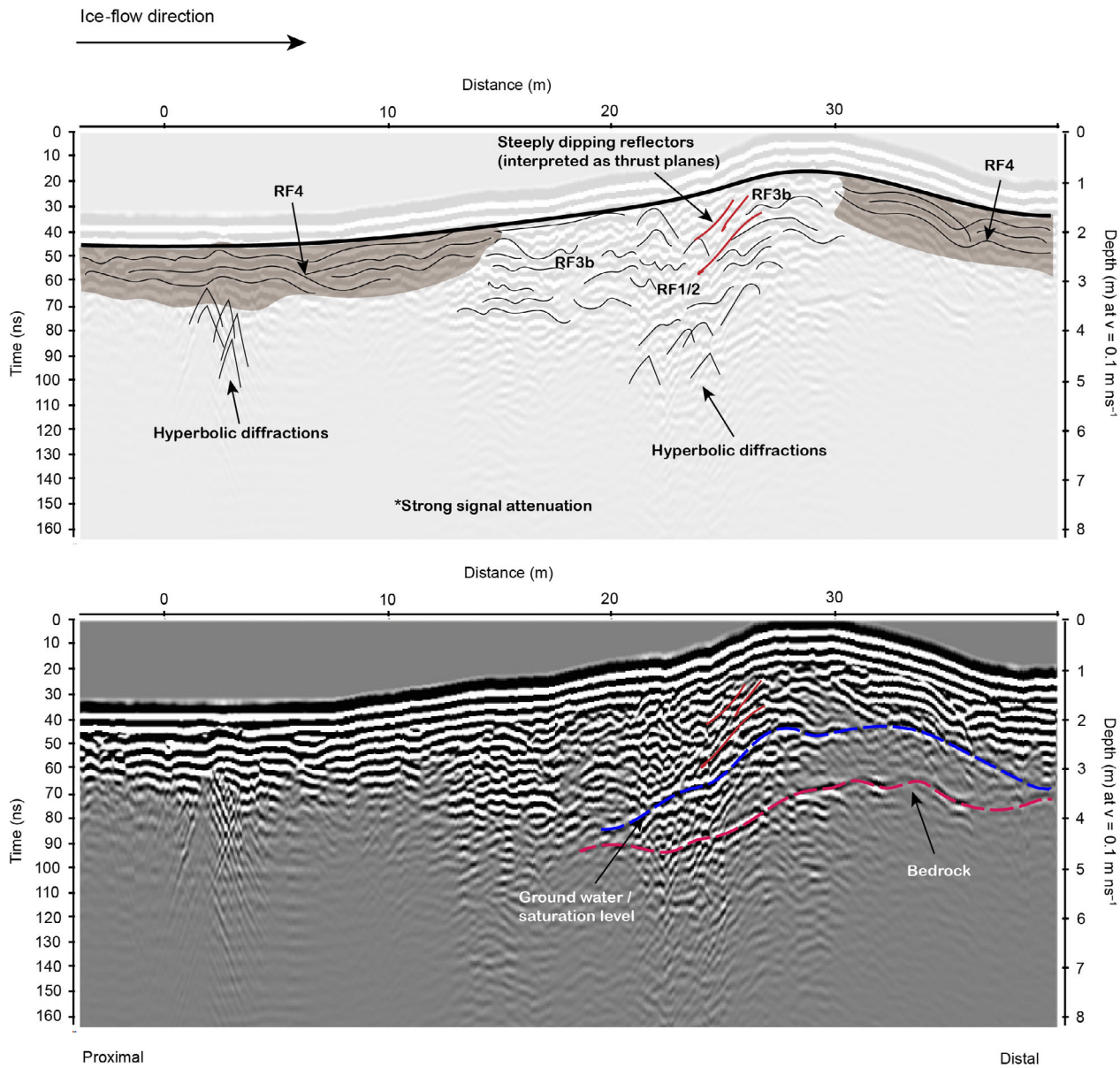


Fig. 15. Radargram #1 acquired at Kurajoki, Porkka (GPR profiles #2 and #3 are presented in Figs S15, S16). Identified radar facies and connected lithofacies are detailed in Table 1.

example, if deposits are formed during summer when meltwater discharge is high, the deposits may be coarser in texture and the size of the unit may be greater as observed in UT2. Moreover, if the ice margin is unstable in a state of calving/retreat deposits may be subject to less proximal compaction than would be expected from a more stable advancing ice margin.

When comparing our results to existing models, we must consider the influence of proglacial water depth and local to regional bedrock topography. Lønne & Nemeč (2011) illustrate the variability of grounding line depositional systems relative to water depth. Ice terminating in shallow water (<175 m) tends to be relatively

thin with a low erosional capacity and therefore subglacial influence is largely restricted to the proximal sides of marginal ridges; however, ice protrusion may form and partly, or fully, override deposits. In very shallow water (<50 m), ice advances over a low-relief seabed and any deposits would be easily overridden; therefore, moraines may present a sheet-like geometry. These shallow-water ridges described by Lønne & Nemeč (2011) are similar to our observations and correspond to the shallow proglacial water depths in the study area (Ojala *et al.* 2013). Furthermore, correlations between DGM interdistances and water depth have been found whereby DGM interdistances are

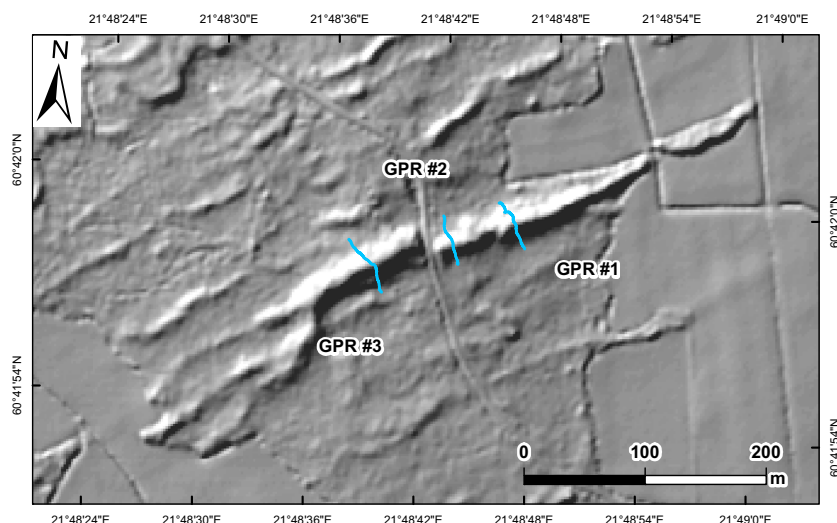


Fig. 16. Hillshaded DEM showing position of GPR profiles along surveyed ridge at Site (4) (DEM source: [®]National Land Survey of Finland, LiDAR digital elevation model, 2/2023).

greater in greater water depths (Ojala 2016). In relation to bedrock topography, the differences in architecture in the Porkka region (Site (3)) demonstrate how bedrock topography influences DGM formation.

Lønne & Nemec (2011) also highlight other factors for consideration, namely the configuration of how well the ice bottom is in contact with the underlying till surface (smooth vs. undulating) and the preservation potential of shallow water deposits due to a limited erosional capacity. These factors can be seen in the existing DGM morphometry study by Rivers *et al.* (2023) whereby DGMs tend to be lower-relief and more laterally continuous when formed in shallow water, and higher-amplitude with greater lateral discontinuity as water depths increase.

Proposed conceptual model

Our results reveal that DGMs situated across southwest Finland are grounding line formations that can vary in size and internal structure depending on the seasonal stage of formation, bedrock topography, sediment availability and water depth. Our field observations do not show evidence of crevasse infilling as a mechanism for DGM formation. Based on our findings and those reported from previous studies, we present an integrated conceptual model whereby DGMs are formed in the same way but with slight variations depending on the seasonal stage of deposition. These variations can be subcategorized as (Fig. 18):

- Summer calving retreat (Fig. 18A, B). Saturated and deformable subglacial sediments are advected toward and deposited at the grounding line via subglacial meltwater and/or extrusion from beneath the margin

during late summer/early autumn. Deposited sediments may be subject to proximal compaction from overriding ice and distal reworkings from proglacial water currents (Bennett & Glasser 2009; Lønne & Nemec 2011). The ice margin subsequently undergoes calving, the grounding line retreats, and the deposited sediments are preserved (Lindén & Möller 2005); calving may lead to loss of buoyancy, which may result in further deformation processes as the margin depresses. After calving, the ice margin may remain stationary or continue to advance, and if enough time allows new sediments will accrue at the margin; however, as the margin is in an unstable state of retreat, the amount of material deposited will likely be less than that during winter advances (Möller 1962). This process would repeat throughout the summer and result in a series of irregularly spaced ridges, which we refer to as intermediate DGM ridges such as UT2 (Rivers *et al.* 2023). As calving processes exert significant forcing over grounding line position resulting in an unstable ice margin (Haseloff & Sergienko 2022), summer ridges would be smaller and more reflective of grounding line forcing dynamics such as water depth relative to ice thickness (Simkins *et al.* 2018).

- Winter and spring push advance (Fig. 18C, D). Saturated and deformable subglacial sediments are advected toward and deposited at the grounding line via subglacial meltwater during late summer/early autumn (e.g. the same processes occurring in summer calving retreat processes). During winter/early spring, however, the ice margin re-advances (Boulton 1986; Ottesen & Dowdeswell 2006), depositing additional material at the grounding line via bulldozing and deforming pre-existing material (this is represented by

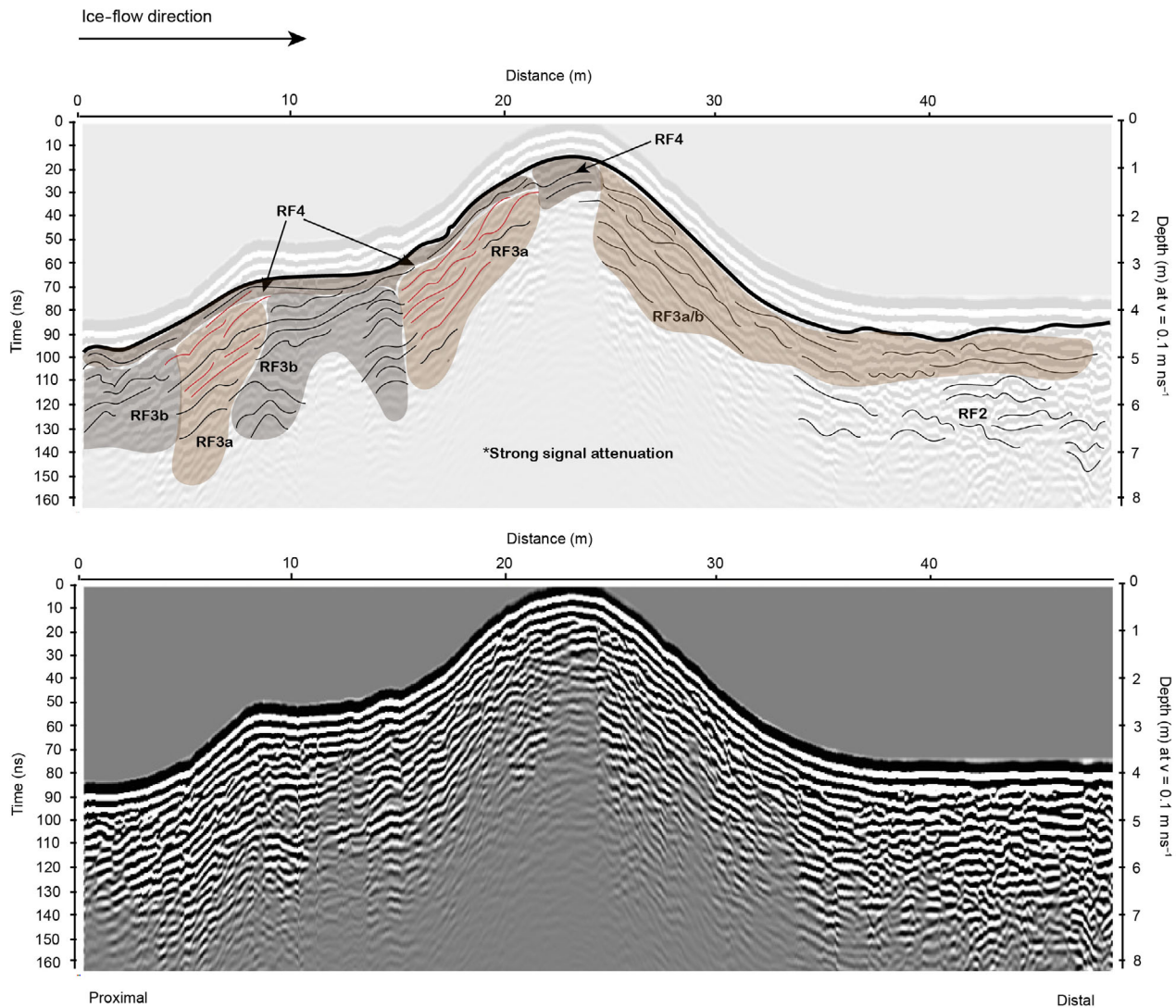


Fig. 17. Radargram #1 from Suorsala, Mynämäki (GPR profiles #2 and #3 are presented in Figs S17, S18). Identified radar facies and connected lithofacies are detailed in Table 1.

the larger Units 3a and 3b), similar to the originally proposed formation by De Geer (1940). This results in a larger, more continuous ridge that is likely formed once per season; however, it should be considered that size and lateral continuity would inevitably be determined by other factors such as ice-moraine contact configuration, water depth and sediment availability (Lønne & Nemeč 2011). These ridges, such as UT1, are considered as regular, prominent DGMs. Furthermore, as the ridge is formed via winter push processes, the position of the ridge would relate more closely to mass balance compared to the grounding line dynamics of summer calving ridges. As ice continues to retreat, a series of similarly formed winter and summer ridges are preserved on the landscape (Fig. 18E).

The differences in depositional processes between different DGMs gives rise to a potential ambiguity regarding the term ‘De Geer moraine’. Lundqvist (2000) pointed out that the term ‘De Geer moraine’ is often extended to similar landforms (e.g. cross-valley moraines, washboard moraines), and even when the term ‘De Geer moraine’ is used very strictly (e.g. only for those moraines originally described by Gerard De Geer), there can be more than one formation mechanism. In contrast, Bouvier *et al.* (2015) suggested that DGMs are an example of equifinality. Ojala (2016) classified De Geer moraine fields into five maturity classes based on their spatial regularity and distinct ridge-type appearance. Given that the term De Geer moraine is thus neither strictly descriptive, nor genetic, we propose that these distinctive fields of ice-marginal ridges could be called

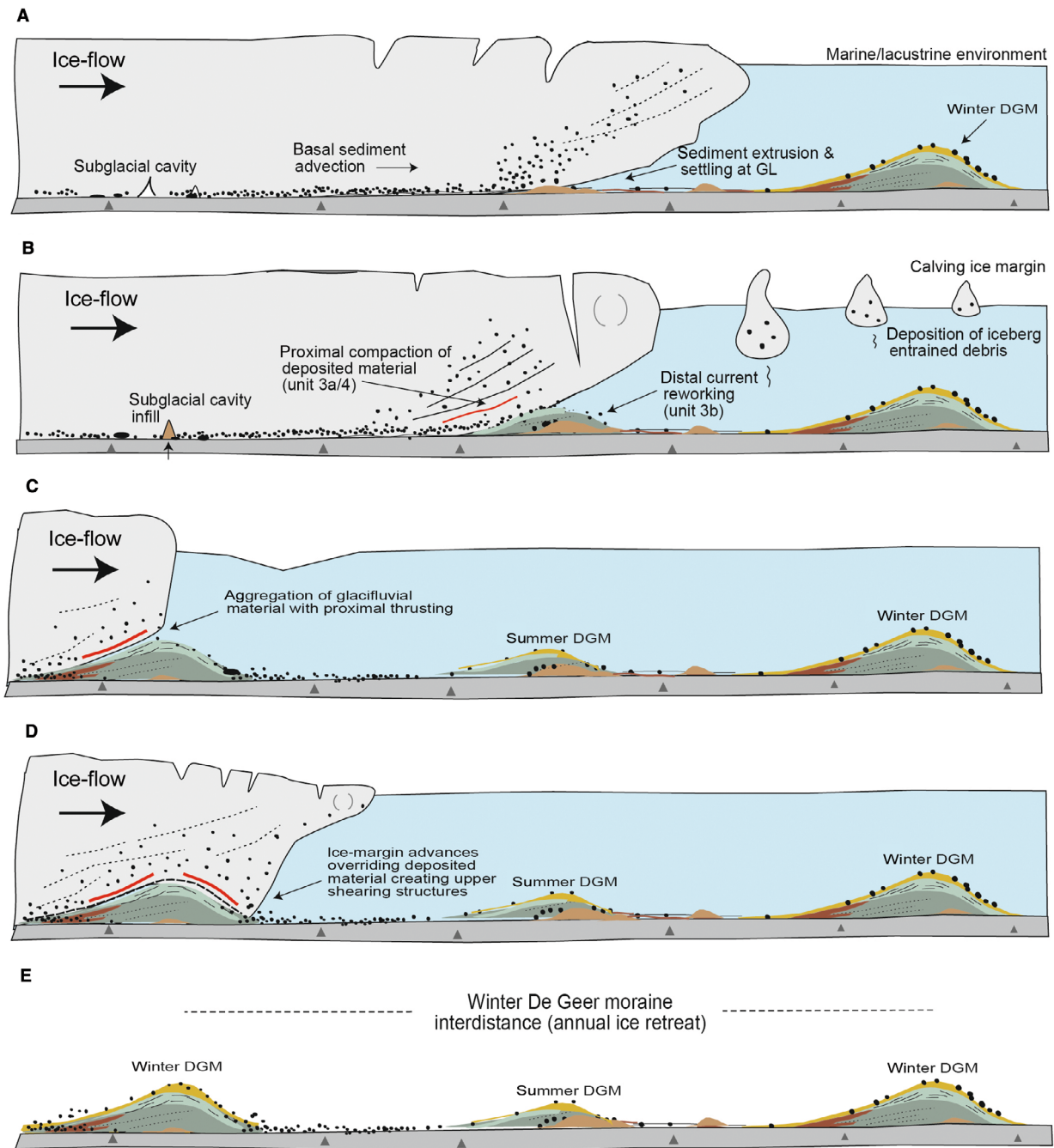


Fig. 18. Proposed conceptual model of inter-seasonal De Geer ridge forming processes. **A.** Late spring/early summer: fine-grained materials settle out at GL (Unit 2). Ice may depress into the bed during temporary stabilizations resulting in coarser-grained sediment extrusion (Unit 3). **B.** Late summer/early autumn: increased subglacial meltwater transports coarser-grained material to the grounding line. Possible proximal compaction may occur due to buoyant flexure of overriding ice (Units 3a/4). Calving processes occur creating a series of irregularly spaced ridges. **C.** Late autumn/early winter: ice margin retreated to winter position. Aggregation of glacial material at grounding line. Possible proximal compaction from buoyant flexure of overriding ice. Release of debris from overriding ice. **D.** Late winter/early spring: ice re-advance over deposited material. Proximal thrusting and significant shearing deform most notably upper proximal units of ridge (Units 4/5); however, deformation could occur throughout sediment package. Release of debris from overriding ice. **E.** 'De Geer terrain' characterized by regular (winter) and irregular (summer) ridges. Interdistances between winter ridges indicate annual rate of retreat.

'De Geer terrain (DGT)'. We believe this captures the equifinality of DGMs and the range of landforms described based on their appearance (fields of parallel

ridges resembling a washboard), whereby different inter-seasonal ridge forming processes may occur within the same environment.

When viewing our integrated model, wider DGT configuration can be considered. As previously highlighted (Fig. 2), DGT can be configured in one of three ways: (i) only regular ridges, (ii) regular ridges interspersed with irregular ridges, or (iii) only irregular ridges. Based on this model, DGT configuration would elucidate which inter-seasonal ridge forming processes are most dominant relative to grounding line dynamics (Lønne & Nemeč 2011). For example, DGT comprising only lower amplitude irregular ridges may suggest that calving processes are most dominant and thus signify increased water depths (Simkins *et al.* 2018). This is not to suggest that evidence of winter re-advance deposits is absent, rather that summer calving is more prominent and therefore ridges of this origin are more plentiful. Equally, the reverse would be true of DGT characterized by more prominent regular ridges, suggesting that calving processes are limited, or pre-existing summer ridges have been destroyed, and therefore assemblages are more indicative of regular winter re-advance deposits. It should be acknowledged that this is a general rule for De Geer ridge formation, and additional local complexities such as bedrock topography may impose significant influences over formation processes.

Implications for ice-marginal reconstructions

As defined in our model, we find that DGT assemblages may contain bi-seasonal signals that may in some instances be identified by the size and regularity of the ridges. This signifies that an annual signal is present; however, the annual regularity of ridges must be carefully identified when considering whether they can be used as annual ice-marginal indicators. As highlighted in previous studies, the variability in DGT appearance and distribution supports the notion that no single model is appropriate for the genesis of all De Geer ridges (Ojala 2016). It would be reasonable to assume that the regularity of ridges in DGT provides some guidance to distinguish between inter-seasonal signals (e.g. regularly spaced ridges are likely to be more indicative of winter re-advances); however, external influences must also be accounted for such as: calving intensity, bedrock topography, sediment availability, ice-moraine contact, water depth etc. Regardless of formation process, both winter push and summer calving ridges denote ice margin spatial positioning. However, for use as retreat rate indicators, the seasonal timing of deposition must be identified.

Previous studies have attempted to address this problem, finding positive correlations between regularly spaced push ridges and annual rates of retreat (De Geer 1940; Bouvier *et al.* 2015; Ojala 2016; Sinclair *et al.* 2018). However, the slight variations between inter-seasonal formation processes can make this correlation difficult to establish (Hoppe 1959; Möller 1962; Zilliacus 1981, 1989; Sollid 1989; Lindén & Möller 2005). Our

study provides an integrated conceptual model for the different seasonal types of De Geer ridge that can form in a grounding line/calving environment. We suggest that future work could use this model to begin to reconstruct detailed ice margin behaviour in Finland.

Conclusions

DGMs may act as valuable ice-marginal indicators. However, to date, their variable mode of formation has presented challenges for this utility. This study develops upon existing morphometry studies, using sedimentological and GPR methods, to refine our understanding of how DGMs are formed. More specifically, this study compares the internal structures of regular and irregular DGMs, revealing that subtly different ridge forming processes can occur within the same environment.

The DGMs studied suggest an overall multi-phase structure, with lower units representing ice-marginal extrusion and/or basal cavity infill deposits, truncated by a larger prominent push/bulldozed unit, which is subsequently deformed by overriding ice. Significant disparities between proximal and distal structures are notable, with proximal parts characterized by laminae, stratification and thrust planes, and distal parts characterized by looser diamicton and erosional effects caused by local topography, calving processes and current reworkings. Generally, the internal architecture of both prominent and intermediate ridges is the same; however, the main architectural differences observed are the extent of Unit 2, which is more extensive in the observed intermediate ridges, as well as the presence of proximally located deformed clays within prominent ridges likely deposited during quiescent periods in winter. We do not see any evidence for crevasse infilling as a mechanism for DGM formation.

We present an integrated conceptual model whereby all De Geer ridges are formed in the same way with slightly different inter-seasonal formation processes occurring within the same sub-aqueous ice-marginal environment. These slight variations can be subcategorized as: (i) sediment deposition at an unstable margin during summer calving, and (ii) sediment bulldozing/pushing at a stabilized margin during a winter re-advance. In addition, we propose a landform classification whereby 'De Geer terrain' may be used as an alternative to 'De Geer moraines' to describe series of parallel ridges arranged in a typical washboard-like configuration. We consider this alternative classification to be helpful and clearer when describing fields of similar ridges that are formed by different inter-seasonal processes.

Previous studies conducted in Sweden have found that prominent, regularly spaced ridges appear to coincide with independently determined margin-retreat rates. We suggest this is an important direction for future research in Finland.

Acknowledgements. – This research is funded by a Ph.D. GTA studentship awarded by Sheffield Hallam University. We kindly thank the Quaternary Research Association for supporting our fieldwork campaign via the QRA New Researcher Award and the Royal Geographical Society via the Monica Cole Grant. For the purposes of open access, the author has applied a Creative Commons Attribution (CC BY) licence to any Author Accepted Manuscript version arising from this submission. We kindly thank Olli Saaristo for allowing us to undertake excavations at Uimarannatie, Haaro, Perniö. We also thank Jan A. Piotrowski for his editorial work, and Mark Johnson and an anonymous reviewer for their thorough reviews of the manuscript. The authors declare that they have no known conflicting interests that could influence the work reported in this paper.

Author contributions. – GER led the writing and editing of this manuscript with input from all authors. All authors contributed to data collection during the fieldwork campaign. Sedimentological analysis was conducted by AEKO, JM and CH. Ground penetrating radar analysis was conducted by GER and RDS. The conceptual model was developed by GER, AEKO, RDS and JM.

Data availability statement. – The data that support the findings of this study are available from the corresponding author upon reasonable request.

References

- Agisoft 2022: Metashape (version 1.8.1). Available at: <https://agisoft.com/downloads/installer/>.
- Andrews, J. T. 1963: End moraines and late glacial chronology in the northern Nain-Okak section of the Labrador coast. *Geografiska Annaler* 45, 158–171, <https://doi.org/10.2307/520391>.
- Beaudry, L. M. & Prichonnet, G. 1991: Late Glacial De Geer moraines with glaciofluvial sediment in the Chapais area, Québec (Canada). *Boreas* 20, 337–394, <https://doi.org/10.1111/j.1502-3885.1991.tb00286.x>.
- Beaudry, L. M. & Prichonnet, G. 1995: Formation of De Geer moraines deposited subglacially, Central Québec. *Géographie Physique et Quaternaire* 49, 337–361, <https://doi.org/10.7202/033059ar>.
- Benn, D. I. & Ballantyne, C. K. 1994: Reconstructing the transport history of glacial sediments; a new approach based on the covariance of clast form indices. *Sedimentary Geology* 91, 215–227, [https://doi.org/10.1016/0037-0738\(94\)90130-9](https://doi.org/10.1016/0037-0738(94)90130-9).
- Benn, D. & Evans, D. J. A. 2010: *Glaciers and Glaciation*. 563 pp. Arnold, London.
- Benn, D. I., Warren, C. R. & Mottram, R. H. 2007: Calving processes and the dynamics of calving glaciers. *Earth-Science Reviews* 82, 143–179, <https://doi.org/10.1016/j.earscirev.2007.02.002>.
- Bennett, M. M. & Glasser, N. F. (eds.) 2009: *Glacial Geology: Ice Sheets and Landforms*. 305 pp. John Wiley & Sons, Chichester.
- Bennett, M. R., Huddart, D. & Waller, R. I. 2000: Glaciofluvial crevasse and conduit fills as indicators of supraglacial dewatering during a surge, Skeiðarárjökull, Iceland. *Journal of Glaciology* 46, 25–34, <https://doi.org/10.3189/172756500781833232>.
- Blake, K. P. 2000: Common origin for De Geer moraines of variable composition in Raudvassdalen, northern Norway. *Journal of Quaternary Science* 15, 633–644, [https://doi.org/10.1002/1099-1417\(200009\)15:6<633::AID-JQS543>3.0.CO;2-F](https://doi.org/10.1002/1099-1417(200009)15:6<633::AID-JQS543>3.0.CO;2-F).
- Boulton, G. S. 1986: Push-moraines and glacier-contact fans in marine and terrestrial environments. *Sedimentology* 33, 677–698, <https://doi.org/10.1111/j.1365-3091.1986.tb01969.x>.
- Boulton, G. S., Smith, G. D. & Morland, L. W. 1984: The reconstruction of former ice sheets and their mass balance characteristics using a non-linearly viscous flow model. *Journal of Glaciology* 30, 140–152, <https://doi.org/10.3189/S0022143000005876>.
- Bouvier, V., Johnson, M. D. & Pässe, T. 2015: Distribution, genesis and annual-origin of De Geer moraines in Sweden: insights revealed by LiDAR. *GFF* 137, 319–333, <https://doi.org/10.1080/11035897.2015.1089933>.
- Clark, C. D. 1997: Reconstructing the evolutionary dynamics of former ice sheets using multi-temporal evidence, remote sensing and GIS. *Quaternary Science Reviews* 16, 1067–1092, [https://doi.org/10.1016/S0277-3791\(97\)00037-1](https://doi.org/10.1016/S0277-3791(97)00037-1).
- Clark, C. D. and 37 others 2022: Growth and retreat of the last British-Irish Ice Sheet, 31 000 to 15 000 years ago: the BRITICH-CHRONO reconstruction. *Boreas* 51, 699–758, <https://doi.org/10.1111/bor.12594>.
- Clark, P. U., Dyke, A. S., Shakun, J. D., Carlson, A. E., Clark, J., Wohlfarth, B., Mitrovica, J. X., Hostetler, S. W. & McCabe, A. M. 2009: The last glacial maximum. *Science* 325, 710–714, <https://doi.org/10.1126/science.1172873>.
- Dalton, A. S., Duffer, H. E., Margold, M., Heyman, J., Clague, J. J., Froese, D. G., Gauthier, M. S., Hughes, A. L. C., Jennings, C. E., Norris, S. L. & Stoker, B. J. 2023: Deglaciation of the north American ice sheet complex in calendar years based on a comprehensive database of chronological data: NADI-1. *Quaternary Science Reviews* 321, 108345, <https://doi.org/10.1016/j.quascirev.2023.108345>.
- De Geer, G. 1889: Ändmoränerna I trakten mellan Spånga och Sundbyberg. *Geologiska Föreningens i Stockholm Förhandlingar* 11, 395–397.
- De Geer, G. 1940: Geochronologia Suecica principes. *Kungliga Svenska Vetenskapsakademiens Handlingar* III, 18, 367 pp.
- Dyke, A. S., Andrews, J. T., Clark, P. U., England, J. H., Miller, G. H., Shaw, J. & Veillette, J. J. 2002: The Laurentide and Innuitian ice sheets during the Last Glacial Maximum. *Quaternary Science Reviews* 21, 9–31, [https://doi.org/10.1016/S0277-3791\(01\)00095-6](https://doi.org/10.1016/S0277-3791(01)00095-6).
- Evans, D. J. A. & Benn, D. I. 2004: *Practical Guide to the Study of Glacial Sediments*. 266 pp. Arnold, London.
- Evans, D. J. A., Phillips, E. R., Hiemstra, J. F. & Auton, C. A. 2006: Subglacial till: formation, sedimentary characteristics and classification. *Earth-Science Reviews* 78, 115–176, <https://doi.org/10.1016/j.earscirev.2006.04.001>.
- Evans, D. J. A., Storrar, R. D. & Rea, B. R. 2016: Crevasse-squeeze ridge corridors: diagnostic features of late-stage palaeo-ice stream activity. *Geomorphology* 258, 40–50, <https://doi.org/10.1016/j.geomorph.2016.01.017>.
- Frödin, G. 1916: Über einige spätglaziale Kalbungsbuchten und fluvioglaziale Estuarien im mittleren Schweden. *Bulletin of the Geological Institution of the University of Upsala* 15, 149–174.
- Glückert, G. 1995: The Salpausselkä end moraines in southwestern Finland. In Ehlers, J., Kozarski, S. & Gibbard, P. (eds.): *Glacial Deposits in North-East Europe*, 51–56. Taylor & Francis Group, London.
- Golledge, N. & Phillips, E. 2008: Sedimentology and architecture of De Geer moraines in western Scottish Highlands, and implications for grounding-line glacier dynamics. *Sedimentary Geology* 208, 1–14, <https://doi.org/10.1016/j.sedgeo.2008.03.009>.
- Gowan, E. J., Zhang, X., Khosravi, S., Rovere, A., Stocchi, P., Hughes, A. L. C., Gyllencreutz, R., Mangerud, J., Svendsen, J.-I. & Lohmann, G. 2021: A new global ice sheet reconstruction for the past 80 000 years. *Nature Communications* 12, 1199, <https://doi.org/10.1038/s41467-021-21469-w>.
- Harrison, D., Ross, N., Russell, A. J. & Jones, S. J. 2022: Ground-penetrating radar (GPR) investigations of a large-scale buried ice-marginal landsystem, Skeiðarársandur, SE Iceland. *Boreas* 51, 824–846, <https://doi.org/10.1111/bor.12587>.
- Haseloff, M. & Sergienko, O. V. 2022: Effects of calving and submarine melting on steady states and stability of buttressed marine ice sheets. *Journal of Glaciology* 68, 1149–1166, <https://doi.org/10.1017/jog.2022.29>.
- Hoppe, G. 1959: Glacial morphology and inland recession in Northern Sweden. *Geografiska Annaler* 41, 193–212.
- Hughes, A. L. C., Gyllencreutz, R., Lohne, Ø. S., Mangerud, J. & Svendsen, J. I. 2016: The last Eurasian ice sheets – a chronological database and time-slice reconstruction, DATED-1. *Boreas* 45, 1–45, <https://doi.org/10.1111/bor.12142>.
- Johansson, P., Lunkka, J. P. & Sarala, P. 2011: Chapter 9 – The glaciation of Finland. *Developments in Quaternary Sciences* 15, 105–116, <https://doi.org/10.1016/B978-0-444-53447-7.00009-X>.

- Jol, H. M. 1995: Ground penetrating radar antennae frequencies and transmitter powers compared for penetration depth, resolution and reflection continuity 1. *Geophysical Prospecting* 43, 693–709, <https://doi.org/10.1111/j.1365-2478.1995.tb00275.x>.
- Jol, H. M. & Bristow, C. S. 2003: GPR in sediments: advice on data collection, basic processing and interpretation, a good practice guide. *Geological Society, London, Special Publications* 211, 9–27.
- Kleman, J., Hättestrand, C., Borgström, I. & Stroeven, A. 1997: Fennoscandian palaeoglaciology reconstructed using a glacial geological inversion model. *Journal of Glaciology* 43, 283–299.
- Lally, A., Ruffell, A., Newton, A. M. W., Rea, B. R., Kahlert, T., Storrar, R. D., Spagnolo, M., Graham, C. & Coleman, M. 2023: The evolution and preservation potential of englacial eskers: an example from Breiðamerkjúkkull, SE Iceland. *Earth Surface Processes and Landforms* 4, 2864–2883, <https://doi.org/10.1002/esp.5664>.
- Larsen, E., Longva, O. & Follestad, B. A. 1991: Formation of De Geer moraines and implications for deglaciation dynamics. *Journal of Quaternary Science* 6, 263–277, <https://doi.org/10.1002/jqs.3390060402>.
- Lindén, M. & Möller, P. 2005: Marginal formation of De Geer moraines and their implications to the dynamics of grounding-line recession. *Journal of Quaternary Science* 20, 113–133, <https://doi.org/10.1002/jqs.902>.
- Livingstone, S. J., Utting, D. J., Ruffell, A., Clark, C. D., Pawley, S., Atkinson, N. & Fowler, A. C. 2017: Discovery of relict subglacial lakes and their geometry and mechanism of drainage. *Nature Communications* 7, ncomms11767, <https://doi.org/10.1038/ncomms11767>.
- Lønne, I. & Nemeč, W. 2011: The kinematics of ancient tidewater ice margins: criteria for recognition from grounding-line moraines. *Ice-Marginal and Periglacial Processes and Sediments. Geological Society, London, Special Publications* 354, 57–75, <https://doi.org/10.1144/SP354.4>.
- Lundqvist, J. 2000: Palaeoseismicity and De Geer Moraines. *Quaternary International* 68–71, 175–186, [https://doi.org/10.1016/S1040-6182\(00\)00042-2](https://doi.org/10.1016/S1040-6182(00)00042-2).
- Lunkka, J., Nikarmaa, T. & Putkinen, N. 2019: Baltic Ice Lake levels and a LiDAR/DEM-based estimate of the glacio-isostatic uplift gradient of the Salpausselkä zone, SE Finland. *Bulletin of the Geological Society of Finland* 91, 119–137, <https://doi.org/10.17741/bgsf/91.1.005>.
- Lunkka, J., Palmu, J.-P. & Seppänen, A. 2021: Deglaciation dynamics of the Scandinavian Ice Sheet in the Salpausselkä zone, southern Finland. *Boreas* 50, 404–418, <https://doi.org/10.1111/bor.12502>.
- Mäkinen, J., Kajuutti, K., Ojala, A. E. K., Ahokangas, E., Tuunainen, A., Valkama, M. & Palmu, J.-P. 2023: Genesis of subglacial triangular-shaped landforms (murtoos) formed by the Fennoscandian Ice Sheet. *Earth Surface Processes and Landforms* 48, 2171–2196, <https://doi.org/10.1002/esp.5606>.
- Möller, H. 1962: Annuella och interannuella ändmoräner. *Geologiska Föreningen I Stockholm Förhandlingar* 84, 134–143, <https://doi.org/10.1080/11035896209449211>.
- Neal, A. 2004: Ground-penetrating radar and its use in sedimentology: principles, problems and progress. *Earth-Science Reviews* 66, 261–330, <https://doi.org/10.1016/j.earscirev.2004.01.004>.
- Ojala, A. E. K. 2016: Appearance of De Geer moraines in southern and western Finland – implications for reconstructing glacier retreat dynamics. *Geomorphology* 255, 16–25, <https://doi.org/10.1016/j.geomorph.2015.12.005>.
- Ojala, A. E. K., Palmu, J.-P., Åberg, A., Åberg, S. & Virkki, H. 2013: Development of an ancient shoreline database to reconstruct the Littorina Sea maximum extension and the highest shoreline of the Baltic Sea basin in Finland. *Bulletin of the Geological Society of Finland* 85, 127–144, <https://doi.org/10.17741/bgsf/85.2.002>.
- Ojala, A. E. K., Putkinen, N., Palmu, J.-P. & Nenonen, K. 2015: Characterization of De Geer moraines in Finland based on LiDAR DEM mapping. *GFF* 137, 304–318, <https://doi.org/10.1080/11035897.2015.1050449>.
- Ottesen, D. & Dowdeswell, J. A. 2006: Assemblages of submarine landforms produced by tidewater glaciers in Svalbard. *Journal of Geophysical Research: Earth Surface* 111, F1, <https://doi.org/10.1029/2005JF000330>.
- Pearce, D., Ely, J., Barr, I. D. & Boston, C. M. 2017: Glacier reconstruction. In *Geomorphological Techniques*, 1–16. British Society for Geomorphology. Available at: <https://e-space.mmu.ac.uk/619301/>.
- Prest, V. K., Grant, D. R. & Rampton, V. N. 1968: Glacial map of Canada. *Geological Survey of Canada, "A" Series Map*, 1253A, <https://doi.org/10.4095/108979>.
- Rainio, H., Saarnisto, M. & Ekman, I. 1995: Younger Dryas end moraines in Finland and NW Russia. *Quaternary International* 28, 179–192, [https://doi.org/10.1016/1040-6182\(95\)00051-J](https://doi.org/10.1016/1040-6182(95)00051-J).
- Rea, B. R. & Evans, D. J. A. 2011: An assessment of surge-induced crevasse and the formation of crevasse squeeze ridges. *Journal of Geophysical Research* 116, F04005, <https://doi.org/10.1029/2011JF001970>.
- Regnéll, C., Becher, G. P., Öhring, C., Greenwood, S. L., Gyllencreutz, R., Blomdin, R., Brendryen, J., Goodfellow, B. W., Mikko, H., Ransed, G. & Smith, C. 2023: Ice-dammed lakes and deglaciation history of the Scandinavian Ice Sheet in central Jämtland, Sweden. *Quaternary Science Reviews* 312, 108219, <https://doi.org/10.1016/j.quascirev.2023.108219>.
- Rinterknecht, V. R., Clark, P. U., Raisbeck, G. M., Yiou, F., Brook, E. J., Tschudi, S. & Lunkka, J. P. 2004: Cosmogenic ¹⁰Be dating of the Salpausselkä I Moraine in southwestern Finland. *Quaternary Science Reviews* 23, 2283–2289, <https://doi.org/10.1016/j.quascirev.2004.06.012>.
- Ritchie, J., Lingle, C., Motyka, R. & Truffer, M. 2008: Seasonal fluctuations in the advance of a tidewater glacier and potential causes: Hubbard Glacier, Alaska, USA. *Journal of Glaciology* 54, 401–411, <https://doi.org/10.3189/002214308785836977>.
- Rivers, G. E., Storrar, R. D., Jones, A. H. & Ojala, A. E. K. 2023: 3D morphometry of De Geer moraines and Crevasse-Squeeze Ridges: differentiating between pushing and squeezing mechanisms from remotely sensed data. *Quaternary Science Reviews* 321C, 108383, <https://doi.org/10.1016/j.quascirev.2023.108383>.
- Saarnisto, M. & Saarinen, T. 2001: Deglaciation chronology of the Scandinavian Ice Sheet from the Lake Omega Basin to the Salpausselkä End Moraines. *Global and Planetary Change* 31, 387–405, [https://doi.org/10.1016/S0921-8181\(01\)00131-x](https://doi.org/10.1016/S0921-8181(01)00131-x).
- Simkins, L. M., Greenwood, S. L. & Anderson, J. B. 2018: Diagnosing ice sheet grounding line stability from landform morphology. *The Cryosphere* 12, 2707–2726, <https://doi.org/10.5194/tc-12-2707-2018>.
- Sinclair, S. N., Licciardi, J. M., Campbell, S. W. & Madore, B. M. 2018: Character and origin of De Geer moraines in the Seacoast region of New Hampshire, USA. *Journal of Quaternary Science* 33, 225–237, <https://doi.org/10.1002/jqs.3017>.
- Sollid, J. L. 1989: Comments on the genesis of De Geer moraines. *Norsk Geografisk Tidsskrift – Norwegian Journal of Geography* 43, 45–47, <https://doi.org/10.1080/00291958908552217>.
- Sollid, J. L. & Carlson, A. B. 1984: De Geer moraines and eskers in Pasvik, North Norway. *Striae* 20, 55–61.
- Stoker, B. J., Livingstone, S. J., Barr, I. D., Ruffell, A., Storrar, R. D. & Roberson, S. 2021: Variations in esker morphology and internal architecture record time-transgressive deposition during ice margin retreat in Northern Ireland. *Proceedings of the Geologists' Association* 132, 409–425, <https://doi.org/10.1016/j.pgeola.2021.03.002>.
- Stokes, C. R., Tarasov, L., Blomdin, R., Cronin, T. M., Fisher, T. G., Gyllencreutz, R., Hättestrand, C., Heyman, J., Hindmarsh, R. C. A., Hughes, A. L. C., Jakobsson, M., Kirchner, N., Livingstone, S. J., Margold, M., Murton, J. B., Noormets, R., Peltier, W. R., Peteet, D. M., Piper, D. J. W., Preusser, F., Renssen, H., Roberts, D., Roche, D. M., Saint-Ange, F., Stroeven, A. P. & Teller, J. T. 2015: On the reconstruction of palaeo-ice sheets: recent advances and future challenges. *Quaternary Science Reviews* 125, 15–49, <https://doi.org/10.1016/j.quascirev.2015.07.016>.
- Stroeven, A. P., Hättestrand, C., Kleman, J., Keyman, J., Fabel, D., Fredin, O., Goodfellow, B. W., Harbor, J. M., Jansen, J. D., Olsen, L., Caffee, M. W., Fink, D., Lundqvist, J., Rosqvist, G. C., Strömberg, B. & Jansson, K. N. 2016: Deglaciation of Fennoscandia. *Quaternary Science Reviews* 147, 91–121, <https://doi.org/10.1016/j.quascirev.2015.09.016>.
- Strömberg, B. 1965: Mappings and geochronological investigations in some moraine areas of South-Central Sweden. *Geografiska Annaler*

- Series A, Physical Geography* 47, 73–82, <https://doi.org/10.1080/04353676.1965.11879715>.
- Svendsen, J. I., Alexanderson, H., Astakhov, V. I., Demidov, I., Dowdeswell, J. A., Funder, S., Gataullin, V., Henriksen, M., Hjort, C., Houmark-Nielsen, M., Hubberten, H. W., Ingólfsson, Ó., Jakobsson, M., Kjær, K. H., Larsen, E., Lokrantz, H., Lunkka, J. P., Lysä, A., Mangerud, J., Matiouchkov, A. & Stein, R. 2004: Late Quaternary ice sheet history of northern Eurasia. *Quaternary Science Reviews* 23, 1229–1271, <https://doi.org/10.1016/j.quascirev.2003.12.008>.
- Todd, B. J., Valentine, P. C., Longva, O. & Shaw, J. 2007: Glacial landforms on German Bank, Scotian Shelf: evidence for Late Wisconsinan ice-sheet dynamics and implications for the formation of De Geer moraines. *Boreas* 16, 148–169, <https://doi.org/10.1080/03009480600992050>.
- Tschudi, S., Ivy-Ochs, S., Schlüchter, C., Kubik, P. & Rainio, H. 2000: ¹⁰Be dating of Younger Dryas Salpausselkä I formation in Finland. *Boreas* 29, 287–293, <https://doi.org/10.1111/j.1502-3885.2000.tb01211.x>.
- Vollmer, F. W. 2023: Orient Software. Available at: <https://www.frederickvollmer.com/orient/index.html>.
- Zilliacus, H. 1981: De Geer moränerna på Replot och Björkönen I Vasa skärgård [The De Geer moraines on the islands of Replot and Björkönen in the Vasa archipelago, western Finland]. *Terrain* 93, 12–24.
- Zilliacus, H. 1989: Genesis of De Geer moraines in Finland. *Sedimentary Geology* 62, 309–317, [https://doi.org/10.1016/0037-0738\(89\)90121-8](https://doi.org/10.1016/0037-0738(89)90121-8).
- Fig. S5.* Trench locations of grain-size curves for location 1 UT1.
- Fig. S6.* Grain-size curves for location 1 UT1. Diamicton curves shown in black. Sand and gravel curves shown in brown.
- Fig. S7.* Correlation between excavated sediment exposure and neighbouring GPR profile #1 at Site (1) UT2 (Fig. 8A). Comparisons with UT1 show the same lithofacies in the same order within the exposure. This is reflected in the radar facies Table 1, presented in the main manuscript.
- Fig. S8.* Location 1, UT2 GPR Radargram #1.
- Fig. S9.* Location 1, UT2 GPR Radargram #2.
- Fig. S10.* Location 1, UT2 GPR Radargram #3.
- Fig. S11.* Trench locations of grain-size curves for location 1 UT2.
- Fig. S12.* Grain-size curves for location 1 UT2. Diamicton curves shown in black. Sand and gravel curves shown in brown.
- Fig. S13.* Location 2, GPR Radargram #2.
- Fig. S14.* Location 2, GPR Radargram #3.
- Fig. S15.* Location 3, GPR Radargram #2.
- Fig. S16.* Location 3, GPR Radargram #3.
- Fig. S17.* Location 4, GPR Radargram #2.
- Fig. S18.* Location 4, GPR Radargram #3.

Supporting Information

Additional Supporting Information to this article is available at <http://www.boreas.dk>.

- Fig. S1.* Correlation between excavated sediment exposure and neighbouring GPR profile #3 at Site (1) UT1 (Fig. 4A). Radar facies are presented in Table 1 within the main manuscript.
- Fig. S2.* Location 1, UT1 GPR Radargram #1.
- Fig. S3.* Location 1, UT1 GPR Radargram #2.
- Fig. S4.* Location 1, UT1 GPR Radargram #3.